

An Uplink Control Channel Design with Complementary Sequences for Unlicensed Bands

Alphan Şahin, *Member, IEEE*, and Rui Yang, *Member, IEEE*

Abstract—In this paper, two modulation schemes based on complementary sequences (CSs) are proposed for uplink control channels in unlicensed bands. These schemes address high peak-to-average-power ratio (PAPR) under non-contiguous resource allocation in the frequency domain and reduce the maximum PAPR to 3 dB. The first scheme allows the users to transmit a small amount of uplink control information (UCI) such as acknowledgment signals and does not introduce a trade-off between PAPR and co-channel interference (CCI). The second scheme, which enables up to 21 UCI bits for a single user or 11 UCI bits for three users in an interlace, is based on a new theorem introduced in this paper. This theorem leads distinct CSs compatible with a wide variety of resource allocations while capturing the inherent relationship between CSs and Reed-Muller (RM) codes, which makes CSs more useful for practical systems. The numerical results show that the proposed schemes maintain the low-PAPR benefits without increasing the error rate for non-contiguous resource allocations in the frequency domain.

Index Terms—Control channels, complementary sequences, PAPR, Reed-Muller code, OFDM, unlicensed spectrum

I. INTRODUCTION

To improve overall network efficiency and address the rapid increase in data demand, the wireless industry has started to extend 3GPP Long-Term Evolution (LTE) and Fifth Generation (5G) New Radio (NR) for the operation in unlicensed bands [2]–[4]. However, the communication protocols designed for licensed bands need major changes as coexistence assurance is required in the unlicensed bands. To ensure fairness of channel access and usage among different radio access technologies, stringent regulatory requirements are imposed on unlicensed bands. For example, according to the ETSI regulations [5], in the 5 GHz band, the power spectral density (PSD) of the transmitted signal should be less than 10 dBm/MHz and the occupied channel bandwidth (OCB) should be larger than 80% of the nominal channel bandwidth. Therefore, a narrow bandwidth transmission (e.g., a single physical resource block (PRB) is 180 kHz in LTE) in 20 MHz channel in a 5 GHz unlicensed band does not meet the OCB requirement and limits the coverage range due to the PSD requirement. To be able to increase the transmit power under the PSD constraint while complying with the OCB requirement, 3GPP LTE enhanced licensed-assisted access (eLAA) and NR in unlicensed spectrum (NR-U) have adopted *interlaced transmission* which allocates disperse and non-contiguous PRBs as shown in Figure 1, called *interlace*, in the

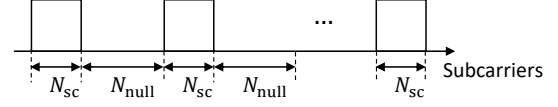


Figure 1. Interlace model.

uplink (UL) [6]. This major change on the baseline resource allocation prohibits the use of single-carrier waveform (e.g., discrete Fourier transform (DFT)-spread orthogonal frequency division multiplexing (OFDM)) and the corresponding physical channels that benefit from low peak-to-average-power ratio (PAPR) in the licensed bands. In addition, the number of utilized PRBs in an interlace in NR is a function of subcarrier spacing and bandwidth, which makes the problem more challenging.

In 3GPP 5G NR R15 [7], the physical uplink control channel (PUCCH) is meticulously designed to ensure the link reliability while handling multiple users with very limited resources for licensed bands. It consists of five different formats. Format 0 is based on sequence selection and designed for 1 or 2 uplink control information (UCI) bits such as acknowledgment (i.e., acknowledgment (ACK) and negative acknowledgment (NACK) signals) or scheduling request (SR). It does not include reference symbols and shares the same structural properties of non-coherent orthogonal signaling [8]. It occupies a single PRB while allowing 6 users to share the same PRB. In [8], an alternative design to Format 0 with reference symbols is discussed. However, no benefit of using reference symbols is observed. Format 1 extends Format 0 to 4-14 OFDM symbols with an orthogonal cover code (OCC). It is based on sequence modulation where a binary phase-shift keying (BPSK) or quadrature phase-shift keying (QPSK) symbol is multiplied with a sequence and includes reference symbols. It supports up to 84 users and provides an enhanced coverage range. For Format 0-1, the reliability is primarily ensured by a set of low-cross correlation seed sequences, in which each sequence results in an OFDM symbol with low PAPR. Orthogonal sequences are generated through cyclic shifts in time by exploiting the properties of unimodular sequences [9]. Format 2-4 support moderate and large UCI payloads. In Format 2, the data symbols and reference symbols are directly mapped to the subcarriers. It occupies 1-2 OFDM symbols and 1-16 PRBs. For Format 3-4, the waveform is based on DFT-spread OFDM to reduce PAPR. Format 3 supports a large payload with 1-16 PRBs with no user multiplexing capacity in the same PRB. On the other hand, Format 4 is limited to a single PRB, but it supports

This paper was presented in part at the IEEE International Conference on Communications (ICC) 2019 [1].

Alphan Şahin and Rui Yang are affiliated with University of South Carolina, Columbia, SC and InterDigital, Huntington Quadrangle, Melville, NY, respectively. E-mail: asahin@mailbox.sc.edu, rui.yang@interdigital.com

up to 4 users in the same PRB with pre-DFT OCC (See Figure 11 in [10]). In 3GPP 5G NR R15, which format is used is determined by the number of assigned symbols and the number of UCI bits to be transmitted. The channel coding is also determined based on the number of UCI bits. While a polar code is adopted for more than 11 bits, a (32,11) linear block code defined in Table 5.3.3.3-1 in [11] is utilized for 3-11 UCI bits.

The PUCCH formats are extended to the interlaced transmission for unlicensed bands in 3GPP 5G NR R16 [6]. To avoid major modifications in the standard, PAPR reduction methods relying on randomization are adopted. For Format 0 and 1, a resource-block dependent sequence generation is utilized, called *cycle-shift hopping*. The cyclic shift used for each PRB in the interlace is determined as a function of the PRB index [12]. Therefore, the coherent additions of the peak samples in time for the same signal component on different PRBs are avoided. Similarly, Format 2 is extended with OCC-cycling across PRBs of an interlace, i.e., a user uses different spreading coefficients for different PRBs. By capturing the user multiplexing feature of Format 4, Format 3 is extended with a pre-DFT OCC with block-wise repetition followed by mapping over the whole interlace in the frequency domain [10]. We refer the reader to [13] and [14] for several other non-standard solutions and discussions for NR PUCCH in the unlicensed band.

The literature is rich with PAPR reduction methods for OFDM [15], [16]. However, low-complexity methods which do not require optimization for each OFDM symbol and tailored for non-contiguous allocation are limited. With DFT precoding and an interleaved subcarrier mapping, an OFDM symbol is converted to a low-PAPR single-carrier waveform with repetitions in time [17]. However, an interleaved subcarrier mapping is not compatible with the interlaces in NR and LTE. In [18], Davis and Jedwab showed that there exists a joint coding and modulation scheme guaranteeing a maximum 3 dB PAPR for OFDM symbols by exploiting complementary sequences (CSs) [19], which utilizes 2^m subcarriers in a contiguous manner, where m is an integer. In [20], a multiple-access scheme based on super-orthogonal convolutional codes utilizing CSs is proposed. By using an interleaved subcarrier mapping, the low-PAPR property of CSs is kept and frequency diversity is achieved. In [21], a theoretical framework is proposed to synthesize CSs with null symbols, i.e., non-contiguous CSs by extending Davis and Jedwab's framework. It can introduce zero elements in CSs of length $2^m \cdot N$ for non-negative integer m and N and the number of non-zero clusters is 2^m . Thus, it does not address NR-U interlaces as the number of PRBs in NR-U interlace (e.g., 10 PRB for 15 kHz) cannot be factorized as 2^m . To the best of our knowledge, a systematic design of low-PAPR communication schemes for flexible interlaced transmission is not available in the literature.

In this study, we propose two modulation schemes for uplink control channel based on non-contiguous CSs. We focus on reliable low data rate communication schemes with resources shared by multiple users for a single OFDM symbol. The first modulation scheme is for 1 or 2 UCI bits and an alternative to NR PUCCH Format 0 for the interlaced transmission. The

second one is a joint coding-and-modulation scheme allows users to transmit moderate payloads in an interlace.

Our main contributions are as follows:

- **Theoretical framework:** To derive the proposed methods, we introduce Theorem 1 and Theorem 2 which allows synthesizing a large number of distinct non-contiguous CSs by permuting the multiple seed Golay complementary pairs (GCPs) systematically.
- **High reliability:** We propose schemes that lead to OFDM symbols with a maximum 3 dB PAPRs while exploiting the frequency diversity. Approximately 3 dB and 4 dB PAPR gains are obtained as compared to the approaches used for NR PUCCH Format 0 and Format 3 without sacrificing the error rate, respectively. A GCP set with low peak cross-correlation is also proposed.
- **Flexible interlace:** We show that there exist low-PAPR modulation schemes for a flexible interlaced transmission. Even if the number of PRBs or the number of zeros between the PRBs in an interlace is changed, the PAPR does not exceed 3 dB with the proposed schemes.
- **Low-complexity design:** The introduced modulation schemes do not rely on symbol-based optimization. Hence, it is suitable for practical systems.
- **Multi-user support:** While the first scheme supports up to 6 users, the second scheme enables 21 UCI bits for a single user or 11 UCI bits for three users on the same interlace of a single OFDM symbol.

The rest of the paper is organized as follows. In Section II, we provide the notation and preliminary discussions. In Section III, we obtain Theorem 1 and Theorem 2. In Section IV, we derive the proposed schemes. In Section V, we compare the proposed schemes with the other state-of-the-art approaches, numerically. We conclude the paper in Section VI.

Notation: The field of complex numbers, the set of integers, the set of positive integers, and the set of non-negative integers are denoted by \mathbb{C} , \mathbb{Z} , \mathbb{Z}^+ , and \mathbb{Z}_0^+ respectively. The symbols i , j , $+$, and $-$ denote $\sqrt{-1}$, $-\sqrt{-1}$, 1, and -1 , respectively. A sequence of length N is represented by $\mathbf{a} = (a_n)_{n=0}^{N-1}$. The element-wise complex conjugation and the element-wise absolute operation are denoted by $(\cdot)^*$ and $|\cdot|$, respectively. The sequence $\tilde{\mathbf{a}}$ is the conjugate of the element-wise reversed sequence \mathbf{a} . The operation $\uparrow_k \{\mathbf{a}\}$ introduces $k-1$ zero symbols between the elements of \mathbf{a} . The operations $\mathbf{a} + \mathbf{b}$, $\mathbf{a} - \mathbf{b}$, $\mathbf{a} \odot \mathbf{b}$, $\mathbf{a} * \mathbf{b}$, and $\langle \mathbf{a}, \mathbf{b} \rangle$ are the element-wise summation, the element-wise subtraction, the element-wise multiplication, linear convolution, and the inner product of \mathbf{a} and \mathbf{b} , respectively.

II. PRELIMINARIES AND FURTHER NOTATION

We model an interlace as a non-contiguous resource allocation which consists of N_{rb} PRBs where the PRBs are separated by N_{null} tones in the frequency domain as illustrated in Figure 1. We assume that each PRB is composed of N_{sc} subcarriers. For example, an interlace in NR-U can be expressed as $N_{\text{sc}} = 12$ subcarriers, $N_{\text{rb}} = 10$ PRBs, and $N_{\text{null}} = 9 \times 12 = 108$ subcarriers for 15 kHz subcarrier spacing. The interlace structure in NR-U varies based on the subcarrier spacing and bandwidth [6].

A. Polynomial Representation of a Sequence

The polynomial representation of the sequence \mathbf{a} can be given by

$$p_{\mathbf{a}}(z) \triangleq a_{N-1}z^{N-1} + a_{N-2}z^{N-2} + \dots + a_0, \quad (1)$$

where $z \in \mathbb{C}$ is a complex number. One can show that the following identities hold true:

$$\begin{aligned} p_{\mathbf{a}}(z^k) &= p_{\uparrow_k\{\mathbf{a}\}}(z), \\ p_{\mathbf{a}}(z^k)p_{\mathbf{b}}(z^l) &= p_{\uparrow_k\{\mathbf{a}\} * \uparrow_l\{\mathbf{b}\}}(z), \\ p_{\mathbf{a}}(z)z^d &= p_{\underbrace{(0, 0, \dots, 0, \mathbf{a})}_d}(z), \end{aligned}$$

for $l, k \in \mathbb{Z}^+$ and $d \in \mathbb{Z}_0^+$. If a sequence consists of zero elements between two non-zero elements, it is a non-contiguous sequence. Otherwise, it is a contiguous sequence. The support of \mathbf{a} is $\{x \in \mathbb{Z}_N | a_x \neq 0\}$. The set $\{a_x | a_x \neq 0, a_i = a_j = 0, x \in \{i+1, i+2, \dots, j-1\}\}$ is denoted as a non-zero cluster in \mathbf{a} .

The polynomial representation given in (1) corresponds to an OFDM symbol in continuous for $z \in \{e^{j\frac{2\pi t}{T_s}} | 0 \leq t < T_s\}$, where T_s denotes the OFDM symbol duration. The instantaneous envelope power can be expressed as

$$|p_{\mathbf{a}}(z)|^2 = \rho_{\mathbf{a}}^+(0) + 2 \sum_{\tau=1}^{N-1} |\rho_{\mathbf{a}}^+(\tau)| \cos\left(\frac{2\pi t}{T_s}\tau + \angle\rho_{\mathbf{a}}(\tau)\right), \quad (2)$$

where $\rho_{\mathbf{a}}^+(\tau) = \sum_{i=0}^{N-\tau-1} a_i^* a_{i+\tau}$ is the aperiodic auto correlation (APAC) of the sequence \mathbf{a} [21].

The minimization of the instantaneous envelope power of an OFDM symbol generated through a non-contiguous sequence in the frequency domain is more constrained as compared to the one with a contiguous sequence. For example, consider the interlace model given in Figure 1. If the same number of non-zero elements in an interlace is utilized contiguously in the frequency domain, the number of constraints that need to be met for 0 dB PAPR (i.e., $\rho_{\mathbf{a}}^+(\tau) = 0$ for $\tau \neq 0$) is $N_{\text{rb}}N_{\text{sc}} - 1$ based on (2). On the other hand, for $N_{\text{null}} \geq N_{\text{sc}}$, the number of constraints increases to $2N_{\text{rb}}N_{\text{sc}} - N_{\text{sc}} - N_{\text{rb}}$. As a numerical example, while the number of constraints for a contiguous resource allocation with 120 subcarriers is 119, it increases to 218 for an interlace in NR for 15 kHz subcarrier spacing, which can be more challenging to satisfy for a low-PAPR design.

B. Complementary Sequences

The sequence pair (\mathbf{a}, \mathbf{b}) of length N is called a GCP if

$$\rho_{\mathbf{a}}(\tau) + \rho_{\mathbf{b}}(\tau) = 0, \quad \text{for } \tau \neq 0, \quad (3)$$

where the sequences \mathbf{a} and \mathbf{b} are CSs. By using the definition, one can show that the GCP (\mathbf{a}, \mathbf{b}) satisfies

$$|p_{\mathbf{a}}(z)|^2 + |p_{\mathbf{b}}(z)|^2 \Big|_{z=e^{j\frac{2\pi t}{T_s}}} = \underbrace{\rho_{\mathbf{a}}(0) + \rho_{\mathbf{b}}(0)}_{\text{constant}}. \quad (4)$$

The main property that we inherited from GCPs in this study is that the instantaneous peak power of the corresponding

OFDM signal generated through a CS \mathbf{a} is bounded, i.e., $\max_t |p_{\mathbf{a}}(e^{j\frac{2\pi t}{T_s}})|^2 \leq \rho_{\mathbf{a}}(0) + \rho_{\mathbf{b}}(0)$. Therefore, based on (4), the PAPR of the OFDM signal is less than or equal to $10 \log_{10}(2) \approx 3$ dB if $\rho_{\mathbf{a}}(0) = \rho_{\mathbf{b}}(0)$. For the other properties of GCPs, we refer the reader to the survey given in [22].

C. Unimodular Sequences

Let $\mathbf{x} = (x_0, x_1, \dots, x_{N-1}) \in \mathbb{C}^N$ be a sequence of length N . If $|x_i| = c$ for $i = 0, 1, \dots, N-1$, \mathbf{x} is referred to as a unimodular or constant-amplitude sequence of length N . Without loss of generality, we assume $c = 1$ in this study. For a unimodular sequence \mathbf{x} , one can show that $\langle \mathbf{x} \odot \mathbf{s}_i, \mathbf{x} \odot \mathbf{s}_j \rangle = 0$ if $i \neq j$, where $\mathbf{s}_r = (e^{j\frac{2\pi r}{N} \times 0}, e^{j\frac{2\pi r}{N} \times 1}, \dots, e^{j\frac{2\pi r}{N} \times (N-1)})$ for $r = 0, 1, \dots, N-1$ [9]. Thus, $\{\mathbf{x} \odot \mathbf{s}_r | r = 0, 1, \dots, N-1\}$ is an orthogonal basis where each sequence can be synthesized in an OFDM transmitter with low-complexity operations, i.e., shifting the useful duration of OFDM signal generated through \mathbf{x} in time cyclically. The unimodular sequences are suitable for OCC design, which have been used for increasing the number of users or transmitting more information bits on the same PRBs in both NR [6] and LTE [23].

D. Algebraic Representation of a Sequence

A generalized Boolean function is a function f that maps from $\mathbb{Z}_2^m = \{(x_1, x_2, \dots, x_m) | x_j \in \mathbb{Z}_2\}$ to \mathbb{Z}_H as $f : \mathbb{Z}_2^m \rightarrow \mathbb{Z}_H$ where H is an integer. We associate a sequence \mathbf{f} of length 2^m with the function $f(x_1, x_2, \dots, x_m)$ by listing its values as (x_1, x_2, \dots, x_m) ranges over its 2^m values in lexicographic order (i.e., the most significant bit is x_1). In other words, the $(x+1)$ th element of the sequence \mathbf{f} is equal to $f(x_1, x_2, \dots, x_m)$ where $x = \sum_{j=1}^m x_j 2^{m-j}$. Note that different generalized Boolean functions yield different sequences as each generalized Boolean function can be uniquely expressed as a linear combination of the monomials over \mathbb{Z}_H [18]. For the sake of simplifying the notation, the sequence (x_1, x_2, \dots, x_m) and the function $f(x_1, x_2, \dots, x_m)$ are denoted by \mathbf{x} and $f(\mathbf{x})$, respectively.

III. THEORETICAL FRAMEWORK

In this section, we introduce Theorem 1 and Theorem 2 to generate CSs with flexible support and explain the origin of the proposed schemes in Section IV. Our first theorem generalizes Golay's concatenation and interleaving methods [19] as follows:

Theorem 1. Let (\mathbf{a}, \mathbf{b}) and (\mathbf{c}, \mathbf{d}) be GCPs of length N and M , respectively, $\omega_1, \omega_2 \in \{u : u \in \mathbb{C}, |u| = 1\}$, and $k, l, d \in \mathbb{Z}$. Then, the sequences \mathbf{t} and \mathbf{r} where their polynomial representations are given by

$$p_{\mathbf{t}}(z) = \omega_1 p_{\mathbf{a}}(z^k) p_{\mathbf{c}}(z^l) + \omega_2 p_{\mathbf{b}}(z^k) p_{\mathbf{d}}(z^l) z^d, \quad (5)$$

$$p_{\mathbf{r}}(z) = \omega_1 p_{\mathbf{a}}(z^k) p_{\mathbf{d}}(z^l) - \omega_2 p_{\mathbf{b}}(z^k) p_{\mathbf{c}}(z^l) z^d, \quad (6)$$

construct a GCP.

Proof. Since the sequence pairs (\mathbf{a}, \mathbf{b}) and (\mathbf{c}, \mathbf{d}) are GCPs, by the definition, $|p_{\mathbf{a}}(z)|^2 + |p_{\mathbf{b}}(z)|^2 = C_1$ and $|p_{\mathbf{c}}(z)|^2 + |p_{\mathbf{d}}(z)|^2 = C_2$, where C_1 and C_2 are some constants. Thus,

we need to show that $|p_t(z)|^2 + |p_r(z)|^2$ is also a constant. Since $p_{\bar{a}}(z^k) = p_{a^*}(z^{-k})z^{kN-k}$, $|p_t(z)|^2 + |p_r(z)|^2$ can be calculated as

$$\begin{aligned}
& |p_t(z)|^2 + |p_r(z)|^2 \\
&= (\omega_1 p_a(z^k) p_c(z^l) + \omega_2 p_b(z^k) p_d(z^l) z^d) \\
&\quad \times (\omega_1^* p_{a^*}(z^{-k}) p_{c^*}(z^{-l}) + \omega_2^* p_{b^*}(z^{-k}) p_{d^*}(z^{-l}) z^{-d}) \\
&\quad + (\omega_1 p_a(z^k) p_{\bar{d}}(z^l) - \omega_2 p_b(z^k) p_{\bar{c}}(z^l) z^d) \\
&\quad \times (\omega_1^* p_{a^*}(z^{-k}) p_{\bar{d}^*}(z^{-l}) - \omega_2^* p_{b^*}(z^{-k}) p_{\bar{c}^*}(z^{-l}) z^{-d}) \\
&\stackrel{(a)}{=} p_a(z^k) p_{a^*}(z^{-k}) p_c(z^l) p_{c^*}(z^{-l}) \\
&\quad + p_a(z^k) p_{a^*}(z^{-k}) p_{\bar{d}}(z^l) p_{\bar{d}^*}(z^{-l}) \\
&\quad + p_b(z^k) p_{b^*}(z^{-k}) p_{\bar{c}}(z^l) p_{\bar{c}^*}(z^{-l}) \\
&\quad + p_b(z^k) p_{b^*}(z^{-k}) p_d(z^l) p_{d^*}(z^{-l}) \\
&\stackrel{(b)}{=} (p_a(z^k) p_{a^*}(z^{-k}) + p_b(z^k) p_{b^*}(z^{-k})) \\
&\quad \times (p_c(z^l) p_{c^*}(z^{-l}) + p_d(z^l) p_{d^*}(z^{-l})) = C_1 C_2,
\end{aligned}$$

where (a) follows from $p_{\bar{c}^*}(z^{-l}) p_{\bar{d}}(z^l) = p_c(z^l) p_{d^*}(z^{-l})$ and (b) is because $p_{\bar{c}}(z^l) p_{\bar{c}^*}(z^{-l}) = p_{c^*}(z^{-l}) p_c(z^l)$ and $p_{\bar{d}}(z^l) p_{\bar{d}^*}(z^{-l}) = p_{d^*}(z^{-l}) p_d(z^l)$. \square

Note that the special cases of Theorem 1 are available in earlier work. For example, binary contiguous CSs or multi-level contiguous CSs are discussed when $M = 1$ [22], [24], [25]. However, Theorem 1 also plays a central role for generating non-contiguous CSs which is not widely discussed in the literature. For example, based on the identities given in Section II-A, the factor z^d increases the degree of the polynomial $\omega_2 p_b(z^k) p_d(z^l)$ by d , which yields two clusters in the sequence \mathbf{t} where the number of zeroes between them can be chosen arbitrarily. This is one of key observations that we exploit in this study to limit the PAPR of OFDM symbol for flexible non-contiguous allocations. Similarly, $k > M$ or $l > N$ can generate non-contiguous CSs due to the convolutions of up-sampled sequences.

To support more information bits, it is important to generate distinct CSs. However, Theorem 1 does not show how to generate distinct CSs, systematically. To address this issue, we introduce a new theorem as follows:

Theorem 2. Let $\pi = (\pi_n)_{n=1}^m$ and $\phi = (\phi_n)_{n=1}^m$ be two sequences defined by permutations of $\{1, 2, \dots, m\}$. For any GCP $(\mathbf{c}_n, \mathbf{d}_n)$ of length $M_n \in \mathbb{Z}^+$, $U \in \mathbb{Z}_0^+$, $d_n \in \mathbb{Z}_0^+$, and $c_n, c', c'' \in [0, H)$ for $n = 1, 2, \dots, m$, let

$$c_i(\mathbf{x}) = \frac{H}{2} \sum_{n=1}^{m-1} x_{\pi_n} x_{\pi_{n+1}} + \sum_{n=1}^m c_n x_{\pi_n}, \quad (7)$$

$$\begin{aligned}
p_o(\mathbf{x}, z) &= \prod_{n=1}^{m-1} p_{c_{\phi_n}}(z) ((1 - x_{\pi_n})(1 - x_{\pi_{n+1}}))_2 \\
&\quad + p_{d_{\phi_n}}(z) (x_{\pi_n} (1 - x_{\pi_{n+1}}))_2 \\
&\quad + p_{\bar{d}_{\phi_n}}(z) ((1 - x_{\pi_n}) x_{\pi_{n+1}})_2 \\
&\quad + p_{\bar{c}_{\phi_n}}(z) (x_{\pi_n} x_{\pi_{n+1}})_2, \quad (8)
\end{aligned}$$

and

$$\begin{aligned}
f_i(\mathbf{x}) &= c_i(\mathbf{x}) + c', \\
g_i(\mathbf{x}) &= c_i(\mathbf{x}) + c'', \\
f_o(\mathbf{x}, z) &= p_o(\mathbf{x}, z) (p_{c_{\phi_m}}(z) (1 - x_{\pi_m})_2 + p_{d_{\phi_m}}(z) x_{\pi_m}), \\
g_o(\mathbf{x}, z) &= p_o(\mathbf{x}, z) (p_{\bar{d}_{\phi_m}}(z) (1 - x_{\pi_m})_2 + p_{\bar{c}_{\phi_m}}(z) x_{\pi_m}), \\
f_s(\mathbf{x}) &= \sum_{n=1}^m d_n x_{\pi_n}.
\end{aligned}$$

Then, the sequences \mathbf{t} and \mathbf{r} where their polynomial representations are given by

$$p_t(z) = \sum_{x=0}^{2^m-1} f_o(\mathbf{x}, z) \times \xi^{j f_i(\mathbf{x})} \times z^{f_s(\mathbf{x})+xU}, \quad (9)$$

$$p_r(z) = \sum_{x=0}^{2^m-1} g_o(\mathbf{x}, z) \times \xi^{j g_i(\mathbf{x})} \times z^{f_s(\mathbf{x})+xU} \quad (10)$$

construct a GCP, where $\xi = e^{\frac{2\pi}{H}}$.

The proof of Theorem 2 is given in Appendix A.

Theorem 2 contains the results in [18], [21], and [26]:

- The functions $f_i(\mathbf{x})$ and $g_i(\mathbf{x})$ in Theorem 2 are identical to the ones in [18] for $c_n, c', c'' \in \mathbb{Z}_{2^h}$ and [26] for $c_n, c', c'' \in \mathbb{Z}_H$, where $h \geq 1$ is an integer. It was shown that $f_i(\mathbf{x})$ and $g_i(\mathbf{x})$ yield the codewords in the cosets of the first-order Reed-Muller (RM) code within the second-order RM code where the Hamming distance between two codewords is at least 2^{m-2} .
- The function $f_s(\mathbf{x})$ in Theorem 2 appears in [21] to generate non-contiguous CSs by increasing the degrees of the polynomials in the summands as in (9) and (10). The number of non-zero clusters in the CSs can reach up to 2^m with $f_s(\mathbf{x})$.

On the other hand, Theorem 2 introduces a new term which can be utilized for obtaining the number of non-zero clusters different than 2^m through multiple seed GCPs:

- In Theorem 2, $f_o(\mathbf{x}, z)$ and $g_o(\mathbf{x}, z)$ are the products of m polynomials determined systematically based on the permutations of ϕ and π for $n = 1, 2, \dots, m$ whereas they are generated through a single GCP of length N and are not functions of n in [21]. While ϕ determines the sequences, π defines the order of the sequences in $(f_o(\mathbf{x}, z))_{x=0}^{2^3-1}$.

For example, let $m = 3$, $\pi = (3, 2, 1)$, and $\phi = (1, 2, 3)$. The values of function $f_o(\mathbf{x}, z)$ can be enumerated as

$$\begin{aligned}
(f_o(\mathbf{x}, z))_{x=0}^{2^3-1} &= (p_{c_3}(z) p_{c_2}(z) p_{c_1}(z), p_{c_3}(z) p_{c_2}(z) p_{d_1}(z), \\
&\quad p_{c_3}(z) p_{d_2}(z) p_{\bar{d}_1}(z), p_{c_3}(z) p_{d_2}(z) p_{\bar{c}_1}(z), \\
&\quad p_{d_3}(z) p_{\bar{d}_2}(z) p_{c_1}(z), p_{d_3}(z) p_{\bar{d}_2}(z) p_{d_1}(z), \\
&\quad p_{d_3}(z) p_{\bar{c}_2}(z) p_{\bar{d}_1}(z), p_{d_3}(z) p_{\bar{c}_2}(z) p_{\bar{c}_1}(z)). \quad (11)
\end{aligned}$$

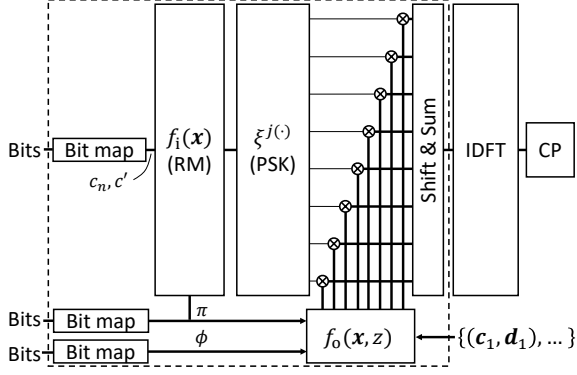


Figure 2. Interpretation of (9) as an OFDM transmitter for $m = 3$.

If ϕ is changed to $(3, 2, 1)$, the enumeration leads to

$$\begin{aligned} (f_o(\mathbf{x}, z))_{x=0}^{2^3-1} = & (p_{c_1}(z)p_{c_2}(z)p_{c_3}(z), p_{c_1}(z)p_{c_2}(z)p_{d_3}(z), \\ & p_{c_1}(z)p_{d_2}(z)p_{\tilde{d}_3}(z), p_{c_1}(z)p_{d_2}(z)p_{\tilde{c}_3}(z), \\ & p_{d_1}(z)p_{\tilde{d}_2}(z)p_{c_3}(z), p_{d_1}(z)p_{\tilde{d}_2}(z)p_{d_3}(z), \\ & p_{d_1}(z)p_{\tilde{c}_2}(z)p_{\tilde{d}_3}(z), p_{d_1}(z)p_{\tilde{c}_2}(z)p_{\tilde{c}_3}(z)) , \end{aligned} \quad (12)$$

where the different sequences are chosen, but their distribution in $(f_o(\mathbf{x}, z))_{x=0}^{2^3-1}$ remains the same as compared to the one in (11). Since $f_o(\mathbf{x}, z)$ is the product of the m polynomials generated through the seed sequences, it is also equal to the polynomial representation of the convolutions of the corresponding sequences based on the identities given in Section II-A. The length of the x th composite sequence after the convolutions can be calculated as $L = (\sum_{n=1}^m M_n) - m + 1$.

For $c_n, c', c'' \in \mathbb{Z}_H$, $f_o(\mathbf{x}, z)$ is multiplied with x th phase-shift keying (PSK) symbol determined by $f_i(\mathbf{x})$, i.e., a RM code over \mathbb{Z}_H in (9). In addition, the degree of the polynomial composed by $f_o(\mathbf{x}, z)$ is also increased by $z^{f_s(\mathbf{x})+xU}$. Therefore, the overall operation can be represented as a shift of the x th phase-rotated composite sequence in the z -domain, where the amount of shift is $f_s(\mathbf{x}) + xU$. Hence, the final sequence \mathbf{t} is then obtained by summing the 2^m shifted and phase-rotated composite sequences. The length of the final sequence can be calculated as $L + U(2^m - 1) + \sum_{n=1}^m d_n$. In Figure 2, we illustrate these steps as an OFDM transmitter with cyclic prefix (CP) where we configure the parameters π , ϕ , c_n , and c' based on information bits.

The number of non-zero elements and the number of non-zero clusters in the CSs are limited to $2^m \cdot N$ and 2^m in [21], respectively. However, they can be chosen more flexibly as a result of polynomial multiplications in $f_o(\mathbf{x}, z)$. To see this, let $\mathbf{c}_n = \uparrow_{k_n} \{\dot{\mathbf{c}}_n\}$ and $\mathbf{d}_n = \uparrow_{k_n} \{\dot{\mathbf{d}}_n\}$ where $(\dot{\mathbf{c}}_n, \dot{\mathbf{d}}_n)$ is a contiguous GCP of length \dot{M}_n . Therefore, $f_o(\mathbf{x}, z)$ is equal to the product of the polynomial representation of upsampled CSs, e.g., $p_{\uparrow_{k_1}\{c_1\}}(z)p_{\uparrow_{k_2}\{c_2\}}(z)p_{\uparrow_{k_3}\{c_3\}}(z)$. Let

$$k_{\kappa_{n+1}} \geq \dot{M}_{\kappa_n} k_{\kappa_n} \quad (13)$$

for $n = 1, 2, \dots, m-1$ and $k_{\kappa_1} \geq 1$, where $\kappa = (\kappa_n)_{n=1}^m$ is a sequence defined by a permutation of $\{1, 2, \dots, m\}$. The seed CSs then spread each other (as Kronecker products) and

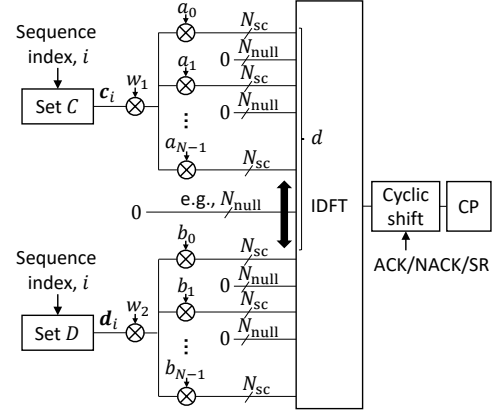


Figure 3. Transmitter for up to 2 UCI bits.

the composite sequences can be non-contiguous. When (13) is tight, the length of the composite sequence is $L = \prod_{n=1}^m \dot{M}_n$.

Let A and B be the number of CSs of length larger than 1 and the number of seed CSs that are not co-linear with each other, respectively. Assuming that the supports of the composite sequences do not overlap in the z -domain, the number of distinct CSs generated with Theorem 2 is $A! \frac{(m!)^2}{(m-B+1)!} H^{m+1}$ under the condition (13) and the presence of at least one seed CS of length larger than 1. This result is substantially different from the numbers provided in [18] and [21]. It can be obtained from $A!$ permutations of κ (i.e., results in different spreading configurations), $m!/(m-B+1)!$ permutations of ϕ (i.e., gives different composite sequences), $m!$ permutations of π (i.e., alters the order of the composite sequence in $(f_o(\mathbf{x}, z))_{x=0}^{2^m-1}$ in the presence of at least one seed GCP, and H different values for $c_{n=1,2,\dots,m}$ and c' . Note that the minimum Euclidean distance for the sequences $\{(\xi^{j f_i(\mathbf{x})})_{x=0}^{2^m-1}\}$ is equal to $2^{m/2} \sin(\pi/H)$ as the codewords are in the second-order RM code. The Boolean functions that determine seed sequences and their positions are also from the second-order RM code. However, the minimum Euclidean distance between CSs is a function of the elements of seed GCPs in general.

IV. CS-BASED UL CONTROL CHANNEL

In this section, we derive two modulation schemes for UCI transmission by relying Theorem 1 and Theorem 2 discussed in Section III. We generate non-contiguous CSs compatible with an interlace through the parameters d , k , and l in Theorem 1 for the first scheme supporting up to 2 UCI bits. We exploit the permutations of π and ϕ , $c_{n=1,2,\dots,m}$, and c' in Theorem 2 to transmit more than 2 UCI bits. We also discuss the user multiplexing with these schemes.

A. Transmission for up to 2 UCI bits

Consider the interlace model in Figure 1. Let $\mathcal{C} \triangleq \{c_1, c_2, \dots, c_K\}$ and $\mathcal{D} \triangleq \{d_1, d_2, \dots, d_K\}$ where (c_i, d_i) is a GCP of length N_{sc} for $i = 1, 2, \dots, K$. We first choose a GCP (\mathbf{a}, \mathbf{b}) of length $N_{rb}/2$ where the elements of \mathbf{a} , \mathbf{b} , \mathbf{c}_i and \mathbf{d}_i are in the set $\mathcal{Q}_1 \triangleq \{+, -, i, j\}$. We then generate

the interlace through (5) in Theorem 1 by setting $\mathbf{c} = \mathbf{c}_i$, $\mathbf{d} = \mathbf{d}_i$, $\omega_1 = \omega_2 = e^{j\frac{\pi}{4}}$, $k = N_{\text{sc}} + N_{\text{null}}$, $l = 1$, and $d = (N_{\text{sc}} + N_{\text{null}}) \times N_{\text{rb}}/2$. With this choice, \mathbf{a} and \mathbf{b} act as sequences spreading \mathbf{c}_i and \mathbf{d}_i . This can be seen from the identities given in Section II-A as

$$p_{\mathbf{a}}(z^{N_{\text{sc}}+N_{\text{null}}})p_{\mathbf{c}}(z) = p_{\uparrow_{N_{\text{sc}}+N_{\text{null}}}\{\mathbf{a}\}*\mathbf{c}}(z), \quad (14)$$

and

$$p_{\mathbf{b}}(z^{N_{\text{sc}}+N_{\text{null}}})p_{\mathbf{d}}(z) = p_{\uparrow_{N_{\text{sc}}+N_{\text{null}}}\{\mathbf{b}\}*\mathbf{d}}(z). \quad (15)$$

In other words, the PRBs are constructed with the phased-rotated versions of \mathbf{c}_i and \mathbf{d}_i and the phase rotations are determined by the elements of \mathbf{a} and \mathbf{b} as shown in Figure 3. Based on the second part of (5) in Theorem 1, d can be chosen as $(N_{\text{sc}} + N_{\text{null}}) \times N_{\text{rb}}/2$ to pad the sequence $\uparrow_{N_{\text{sc}}+N_{\text{null}}}\{\mathbf{b}\}*\mathbf{d}_i$ with $(N_{\text{sc}} + N_{\text{null}}) \times N_{\text{rb}}/2$ zeros. Hence, while the first half of the interlace is a function of \mathbf{a} and \mathbf{c}_i , the second part is generated through \mathbf{b} and \mathbf{d}_i as illustrated in Figure 3. For instance, by considering the interlace parameters in NR-U for 15 kHz subcarrier spacing, the interlace can be constructed when $k = 120$, $l = 1$, and $d = 600$ and the sequences \mathbf{a} , \mathbf{b} , \mathbf{c}_i , \mathbf{d}_i can be arbitrarily chosen such as $\mathbf{a} = (+, +, +, j, i)$, $\mathbf{b} = (+, i, -, +, j)$, $\mathbf{c}_i = (+, +, +, +, -, -, -, +, i, j, -, +)$, and $\mathbf{d}_i = (+, +, i, i, +, +, -, +, +, -, +, -)$ [27].

One of the main benefits of the proposed approach is that \mathcal{C} and \mathcal{D} can be reused by changing N_{null} , d , or defining a new single GCP (\mathbf{a}, \mathbf{b}) , which remarkably simplifies the design involving different interlace configurations. For example, the GCP (\mathbf{a}, \mathbf{b}) can be configured based on subcarrier spacing to maintain signal bandwidth. In another example, a larger d can generate a gap in the frequency domain, which can be utilized for contiguous random access signals. In both examples, PAPR is still maintained to be less than or equal to 3 dB without modifying the sequences in \mathcal{C} and \mathcal{D} . Note that we design \mathcal{C} and \mathcal{D} in Section IV-A3 to address the co-channel interference (CCI) (i.e., inter-cell interference) minimization problem independently of the spreading sequences \mathbf{a} and \mathbf{b} without losing the low-PAPR benefit.

1) *User multiplexing and Transmitter*: For this scheme, we consider orthogonal sequence selection for user multiplexing and UCI transmission. We assume that all scheduled users utilize the i th GCP $(\mathbf{c}_i, \mathbf{d}_i)$ and GCP (\mathbf{a}, \mathbf{b}) . No overhead due to the reference symbols is introduced as in NR PUCCH Format 0. The interlace has $N_{\text{sc}}N_{\text{rb}}$ non-zero elements. Hence, it is possible to generate $N_{\text{sc}}N_{\text{rb}}$ orthogonal resources which can be shared by up to $N_{\text{sc}}N_{\text{rb}}$ users. By exploiting the property of unimodular sequences as discussed in Section II-C, the r th orthogonal resource can be generated by multiplying the ι th non-zero element of the CS with $e^{j\frac{2\pi i}{N_{\text{sc}}N_{\text{rb}}}\times\iota}$ for $r, \iota \in \{0, 1, \dots, N_{\text{sc}}N_{\text{rb}} - 1\}$. However, the orthogonality between the sequences cannot be kept under dispersive channels. To circumvent this issue, the phase rotation is restricted to be periodic with the period of N_{sc} , i.e., $r = \{0, N_{\text{rb}}, 2N_{\text{rb}}, \dots, (N_{\text{sc}} - 1)N_{\text{rb}}\}$. Therefore, the orthogonality *within* the PRB can still be maintained if the channel between each user and the base station is assumed to be flat within the bandwidth of the PRB. Under this restriction, the maximum number of users that can

be supported reduces to N_{sc} , but a low-complexity receiver can be employed. Note that corresponding modulation operation in the frequency domain can be effectively implemented through uniformly separated cyclic shifts in time as shown in Figure 3. If each PRB consists of $N_{\text{sc}} = 12$ subcarriers, 12 orthogonal resources in the interlace can be shared by 6 users to transmit 1-bit information (e.g., ACK/NACK) or 3 users to transmit 2-bit information (e.g., ACK/NACK and scheduling request) with M -ary orthogonal signaling, where $M = 2$ for 1 UCI bit or $M = 4$ for 2 UCI bits. Each user selects one of the orthogonal resources to indicate UCI.

2) *Receiver Design*: The receiver exploits the orthogonality of the sequences in each PRB to decode the information. Since there is no reference symbol, the receiver first calculates the absolute square of the matched filter output for the r th orthogonal sequence in each PRB. It then combines the results for both ACK and NACK at different PRBs to obtain the test statistic. If the test statistic is lower than a threshold determined by Neyman-Pearson criterion, it is considered as discontinuous transmission (DTX), i.e., the user could not decode the signal in the downlink. Otherwise, by comparing the matched filter results, it determines if it is ACK or NACK. Note that the detected sequence can indicate ACK/NACK and/or SR, depending on the network configuration.

3) *Co-channel interference mitigation*: For the CCI minimization, the cross-correlation between any two sequences in \mathcal{C} and \mathcal{D} should be as low as possible. Due to the multipath channel, the signals may be exposed to additional shift in time within the CP. Therefore, the cross-correlation analysis should consider the largest possible correlation in *time*. In the frequency domain, the peak cross-correlation between \mathbf{c}_i and \mathbf{c}_j can be defined as

$$\rho_{\text{peak}}(\mathbf{c}_i, \mathbf{c}_j) \triangleq \max_{r \in [0, N_{\text{sc}}-1]} \langle \mathbf{c}_i, \mathbf{c}_j \odot \mathbf{s}_r \rangle \quad (16)$$

where $\mathbf{s}_r = (e^{j\frac{2\pi i}{N_{\text{sc}}}\times 0}, e^{j\frac{2\pi i}{N_{\text{sc}}}\times 1}, \dots, e^{j\frac{2\pi i}{N_{\text{sc}}}\times (N_{\text{sc}}-1)})$. Therefore, the maximum peak cross-correlation for both sequences in \mathcal{C} and \mathcal{D} should be minimized, i.e., $\rho_{\text{peak}}(\mathbf{c}_i, \mathbf{c}_j) \leq \beta$ and $\rho_{\text{peak}}(\mathbf{d}_i, \mathbf{d}_j) \leq \beta$ for $i \neq j$ and $i, j \in \{1, 2, \dots, K\}$, where β is a threshold. In NR, the number of available base sequences is set to $K = 30$ for $N_{\text{sc}} = 12$ [6] and the maximum peak cross-correlation is 0.8. Hence, we also target the same number of sequences in \mathcal{C} and \mathcal{D} and a similar or better maximum peak cross-correlation with CSs. This naturally leads to the following question for the proposed scheme: Do there exist \mathcal{C} and \mathcal{D} for $K = 30$ and $N_{\text{sc}} = 12$ such that the maximum peak cross-correlation between any two CSs is less than 0.8?

To answer this question, we propose a simple search algorithm which exploits the exhaustively generated GCPs in [27] for length 12 to obtain \mathcal{C} and \mathcal{D} . We initialize the algorithm with $V = 52$ GCPs of length 12 listed in [27] and populate as $\mathcal{S}'_c = \{\mathbf{c}'_1, \dots, \mathbf{c}'_V\}$ and $\mathcal{S}'_d = \{\mathbf{d}'_1, \dots, \mathbf{d}'_V\}$. For the u th seed GCP $(\mathbf{c}'_u, \mathbf{d}'_u)$, we first enumerate $W = 8$ equivalent GCPs by interchanging, reflecting both (i.e., reversing the order of the elements of the sequences), and conjugate reflecting original sequences in the seed GCP, which lead to the sets $\mathcal{S}'_c = \{\mathbf{c}'_1, \dots, \mathbf{c}'_W\}$ and $\mathcal{S}'_d = \{\mathbf{d}'_1, \dots, \mathbf{d}'_W\}$. Because of the properties of GCP, the $(\mathbf{c}'_v, \mathbf{d}'_v)$ still constructs GCPs

Table I
THE SEQUENCES IN \mathcal{C} AND \mathcal{D}

i	\mathbf{c}_i	\mathbf{d}_i
1	(+, -, i, j, +, -, -, +, +, +, +)	(-, +, -, -, +, -, +, j, j, +, +)
2	(+, -, j, i, +, -, -, +, +, +, +)	(-, +, +, +, -, +, +, i, i, +, +)
3	(+, +, +, +, i, +, -, j, +, -, -, +)	(+, +, -, -, i, +, +, i, +, -, -, -)
4	(+, -, -, +, i, -, +, j, +, +, +, +)	(-, +, -, +, j, +, +, j, -, -, +, +)
5	(+, +, +, +, j, +, -, i, +, -, -, +)	(+, +, -, -, j, +, +, j, +, -, -, -)
6	(+, -, -, +, j, -, +, i, +, +, +, +)	(-, +, -, +, i, +, +, i, -, -, +, +)
7	(+, +, +, +, i, -, +, j, +, -, -, +)	(+, +, -, -, i, -, -, i, +, -, -, -)
8	(+, -, -, +, i, +, j, +, +, +, +)	(-, +, -, +, j, -, j, -, -, +, +)
9	(+, +, +, +, j, -, +, i, +, -, -, +)	(+, +, -, -, j, -, j, +, -, -, -)
10	(+, -, -, +, j, +, i, +, +, +, +)	(-, +, -, +, i, -, -, i, -, -, +, +)
11	(+, +, -, +, j, +, j, +, +, +, +)	(-, +, -, j, -, i, -, -, +, +, +)
12	(+, +, -, +, -, i, +, +, +, +, +)	(-, +, -, i, -, j, -, -, +, +, +)
13	(+, +, +, +, i, -, j, +, -, -, -)	(+, +, +, -, j, +, -, -, +, +, +)
14	(+, +, +, +, j, -, i, +, -, -, -)	(+, +, +, -, i, +, -, -, +, +, +)
15	(+, +, +, +, +, j, -, j, +, +, +, +)	(-, +, -, j, +, i, +, -, -, +, +)
16	(+, +, -, +, +, i, -, +, +, +, +)	(-, +, -, i, +, j, +, -, -, +, +)
17	(+, +, -, +, +, +, j, -, +, -, -, -)	(+, +, +, -, j, +, +, -, -, +, +)
18	(+, +, +, +, j, +, i, +, -, -, -)	(+, +, +, -, i, +, +, -, -, +, +)
19	(+, +, +, +, i, +, -, +, +, -, -, -)	(+, +, +, -, -, j, i, -, -, -, -)
20	(+, -, +, +, -, +, j, j, +, +, +, +)	(-, +, -, j, i, -, -, -, +, +, +)
21	(+, +, +, -, j, j, +, +, +, +, +)	(+, +, +, -, +, +, +, i, j, -, -, -, -)
22	(+, -, +, +, +, -, i, i, +, +, +, +)	(-, +, -, i, j, +, +, -, -, +, +)
23	(+, +, +, +, i, -, +, -, +, +, +, +)	(+, +, +, i, -, +, +, +, j, -, -, -, -)
24	(+, +, +, j, -, +, -, +, +, +, +)	(+, +, +, j, -, +, +, +, +, -, -, -)
25	(+, +, -, +, +, +, j, i, -, -, -)	(+, +, -, +, j, +, +, -, -, +, +)
26	(+, -, -, j, i, +, +, +, +, +, +)	(-, +, +, +, -, +, i, +, +, +, +)
27	(+, +, +, +, -, +, -, i, j, -, -, -, -)	(+, +, +, +, i, i, -, +, +, +, +)
28	(+, -, -, i, j, -, -, +, -, +, +)	(-, +, +, +, -, +, j, +, -, +, +)
29	(+, +, -, +, i, +, -, +, -, +, +)	(+, +, -, +, i, +, +, j, +, -, -, -)
30	(+, +, -, +, j, -, +, j, +, +, +)	(-, +, +, +, i, +, +, j, +, -, +)

for $\dot{v} = 1, \dots, W$. For a given candidate GCP $(\mathbf{c}'_{\dot{v}}, \mathbf{d}'_{\dot{v}})$, we calculate $\langle \mathbf{c}_i, \mathbf{c}'_{\dot{v}} \odot \mathbf{s}_r \rangle$ and $\langle \mathbf{d}_i, \mathbf{d}'_{\dot{v}} \odot \mathbf{s}_r \rangle$ for $\mathbf{c}_i \in \mathcal{C}$ and $\mathbf{d}_i \in \mathcal{D}$ and $r \in \{0, 1/Mu, \dots, (Mu-1)/Mu\}$ and $u > 1$. If the results are less than or equal to β for all r , we update \mathcal{C} and \mathcal{D} by including the sequences in the candidate GCP to the sets.

We list the sets obtained for \mathbf{c}_i and \mathbf{d}_i in Table I for $\beta = 0.715$ and $u = 128$. With the aforementioned procedure, we could not obtain \mathcal{C} and \mathcal{D} when $\beta < 0.715$ for $K = 30$ and $N_{sc} = 12$. However, the numerical results given in Section V show that the maximum peak cross-correlation is still less than the ones for Zadoff-Chu (ZC) sequences and the sequences adopted in NR [6]. In [28], a comparison for the peak cross-correlation for different sequences sets is provided. The comparison shows that reducing maximum peak cross-correlation less than 0.7 is challenging under PAPR and QPSK alphabet constraints. It is also worth noting that the sets obtained for \mathbf{c}_i and \mathbf{d}_i are not unique and are based on the initial seed sequences.

B. Transmission for more than 2 UCI bits

In NR, N_{sc} is fixed to $12 = 2^2 \times 3$ subcarriers. Assuming an even number of non-zero clusters, e.g., $N_{rb} = 10$ clusters, we set $m = 3$. Let (\mathbf{a}, \mathbf{b}) be a GCP of length 3, and (\mathbf{c}, \mathbf{d}) be a GCP of length $N_{rb}/2$. Based on Theorem 2, the following configurations result in CSs compatible with the interlace in Figure 1:

- Configuration 1: $(\mathbf{c}_1, \mathbf{d}_1) = ((+), (+))$, $(\mathbf{c}_2, \mathbf{d}_2) = (\mathbf{a}, \mathbf{b})$, $(\mathbf{c}_3, \mathbf{d}_3) = (\uparrow_{2(N_{null}+N_{sc})} \{\mathbf{c}\}, \uparrow_{2(N_{null}+N_{sc})} \{\mathbf{d}\})$, $U = 3$, $d_{\pi_n=1} = N_{null} + N_{sc} - 4U$, and $d_{\pi_n \neq 1} = 0$

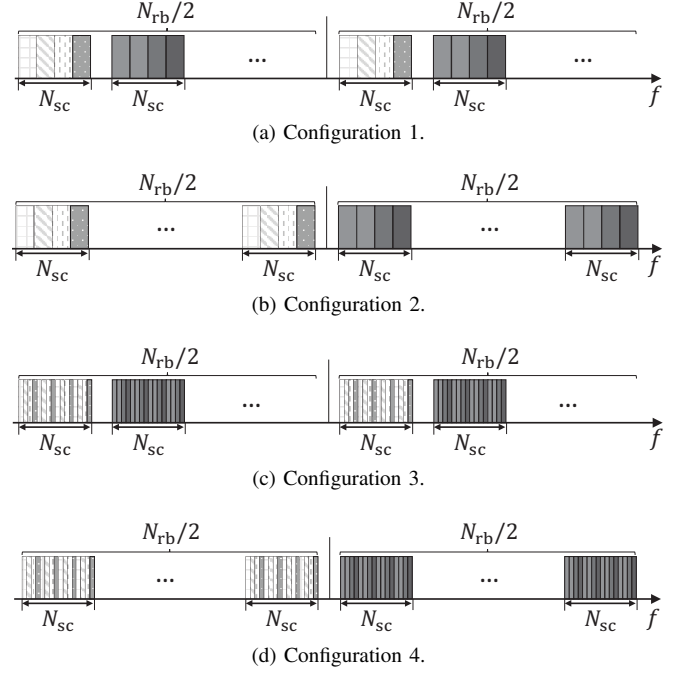


Figure 4. Configurations. Each color tone represents one of the 2^3 QPSK symbols distributed to PRBs through \mathbf{a} , \mathbf{b} , $\tilde{\mathbf{a}}$, and $\tilde{\mathbf{b}}$ of length 3.

- Configuration 2: $(\mathbf{c}_1, \mathbf{d}_1) = ((+), (+))$, $(\mathbf{c}_2, \mathbf{d}_2) = (\mathbf{a}, \mathbf{b})$, $(\mathbf{c}_3, \mathbf{d}_3) = (\uparrow_{N_{null}+N_{sc}} \{\mathbf{c}\}, \uparrow_{N_{null}+N_{sc}} \{\mathbf{d}\})$, $U = 3$, $d_{\pi_n=1} = (N_{null} + N_{sc})N_{rb}/2 - 4U$, and $d_{\pi_n \neq 1} = 0$
- Configuration 3: $(\mathbf{c}_1, \mathbf{d}_1) = ((+), (+))$, $(\mathbf{c}_2, \mathbf{d}_2) = (\uparrow_4 \{\mathbf{a}\}, \uparrow_4 \{\mathbf{b}\})$, $(\mathbf{c}_3, \mathbf{d}_3) = (\uparrow_{2(N_{null}+N_{sc})} \{\mathbf{c}\}, \uparrow_{2(N_{null}+N_{sc})} \{\mathbf{d}\})$, $U = 1$, $d_{\pi_n=1} = N_{null} + N_{sc} - 4U$, and $d_{\pi_n \neq 1} = 0$
- Configuration 4: $(\mathbf{c}_1, \mathbf{d}_1) = ((+), (+))$, $(\mathbf{c}_2, \mathbf{d}_2) = (\uparrow_4 \{\mathbf{a}\}, \uparrow_4 \{\mathbf{b}\})$, $(\mathbf{c}_3, \mathbf{d}_3) = (\uparrow_{N_{null}+N_{sc}} \{\mathbf{c}\}, \uparrow_{N_{null}+N_{sc}} \{\mathbf{d}\})$, $U = 1$, $d_{\pi_n=1} = (N_{null} + N_{sc})N_{rb}/2 - 4U$, and $d_{\pi_n \neq 1} = 0$

While Configuration 1 and Configuration 2 cascade sequences \mathbf{a} , \mathbf{b} , $\tilde{\mathbf{a}}$, and $\tilde{\mathbf{b}}$ in each PRB, Configuration 3 and Configuration 4 interleave the elements of these sequences. The difference between Configuration 1 and Configuration 2 is that they shuffle the sequences in PRBs in the interlace in a different order because of the choices of up-sampling factors and $d_{\pi_n=1}$. Similarly, Configuration 3 and Configuration 4 yield different orders in the interlace. For these configurations, \mathbf{a} , \mathbf{b} , $\tilde{\mathbf{a}}$, and $\tilde{\mathbf{b}}$ are multiplied the elements of \mathbf{c} , \mathbf{d} , $\tilde{\mathbf{c}}$, and $\tilde{\mathbf{d}}$ and 2^3 QPSK symbols based on π and ϕ for $H = 4$. The distribution of the QPSK symbols to PRBs for different configurations are illustrated in Figure 4. For all configurations, N_{null} and N_{rb} can be chosen flexibly without concern of increasing the PAPR.

Each configuration leads to $(3!)^2 H^{m+1}$ CSs compatible with the interlace structure in NR-U since the number of seed CSs that are not co-linear B is 3 and $m = 3$. For $H = 4$, it gives 9216 CSs with a QPSK alphabet. By including the distinct combinations of (\mathbf{a}, \mathbf{b}) and (\mathbf{c}, \mathbf{d}) , i.e., interchanging the sequences in a GCP, e.g., (\mathbf{b}, \mathbf{a}) , or conjugate reflecting one of the sequences in a GCP, e.g., $(\tilde{\mathbf{c}}, \mathbf{d})$, the number of distinct CSs increases by a factor 64. Therefore, $\lceil \log_2 64 \times 9216 \rceil = 19$ information bits can be transmitted for each configuration. As

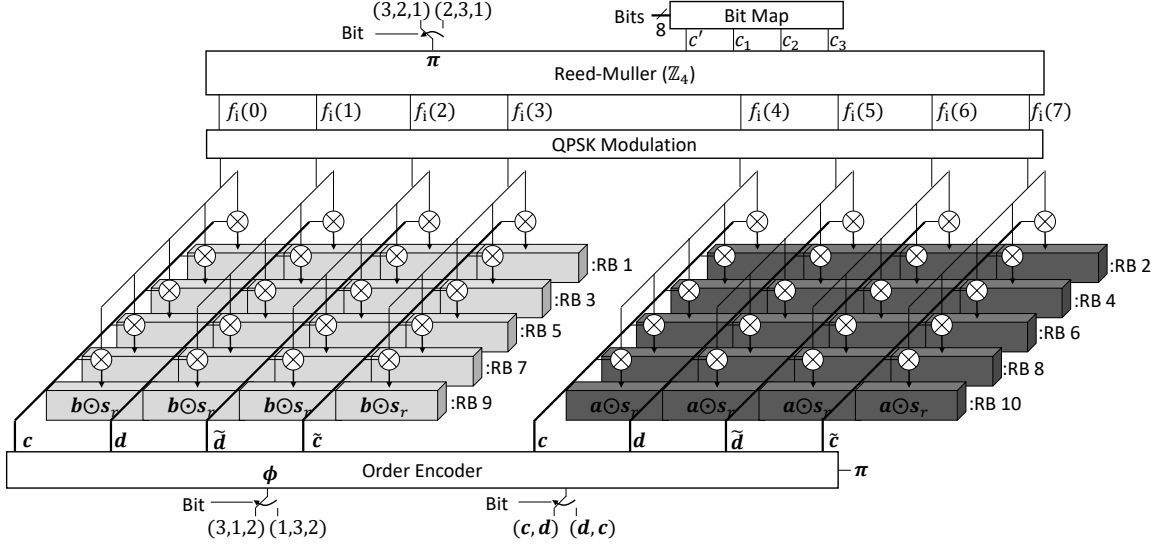


Figure 5. Transmitter for more than 2 UCI bits based on Configuration 1. The phases of \mathbf{a} and \mathbf{b} are modified based on the order encoder and the RM code.

a result, overall, there exist at least $4 \times 64 \times 9216 = 2359296$ CSs, which can carry a maximum of 21 UCI bits.

1) *User multiplexing and Transmitter*: To allow user multiplexing in the interlace while enabling a low-complexity receiver, we keep the orthogonality of the sequences from different users in each PRB. To meet this condition, we exploit the property of the unimodular sequences and consider only one of the configurations, e.g., Configuration 1. We obtain three orthogonal sequences by modulating unimodular \mathbf{a} and \mathbf{b} as $\mathbf{a} \odot \mathbf{s}_r$ and $\mathbf{b} \odot \mathbf{s}_r$, respectively, where $\mathbf{s}_r = (e^{r \frac{2\pi i}{3} \times 0}, e^{r \frac{2\pi i}{3} \times 1}, e^{r \frac{2\pi i}{3} \times 2})$ and $r \in \{0, 1, 2\}$. In addition, we fix the locations of $\mathbf{a} \odot \mathbf{s}_r$ and $\mathbf{b} \odot \mathbf{s}_r$ on each PRB by setting $\phi_{m=3} = 2$ and $\pi_{m=3} = 1$, which result in $\pi \in \{(3, 2, 1), (2, 3, 1)\}$ and $\phi \in \{(3, 1, 2), (1, 3, 2)\}$. The rationale behind this choice can be understood by expressing $f_o(\mathbf{x}, z)$ for $\phi_{m=3} = 2$ and $\pi_{m=3} = 1$ as

$$f_o(\mathbf{x}, z) = p_o(\mathbf{x}, z)(p_{a \odot s}(z)(1 - x_1)_2 + p_{b \odot s}(z)x_1). \quad (17)$$

While $p_o(\mathbf{x}, z)$ takes different values depending on \mathbf{c} , \mathbf{d} , and the first two elements of π and ϕ , the remaining term in (17) places $\mathbf{a} \odot \mathbf{s}$ and $\mathbf{b} \odot \mathbf{s}_r$ in a fixed order. Therefore, the sequences $\mathbf{a} \odot \mathbf{s}_r$ and $\mathbf{b} \odot \mathbf{s}_r$ are multiplied with the elements of \mathbf{c} , \mathbf{d} , $\tilde{\mathbf{c}}$, $\tilde{\mathbf{d}}$ and the outcome of $f_i(\mathbf{x})$. The proposed scheme enables three users to transmit $\log_2(2^2 H^{m+1}) = 10$ bits on the same interlace for a given GCP (\mathbf{c}, \mathbf{d}) . The number of bits can be increased if the seed sequences \mathbf{c} and \mathbf{d} are modified. For example, if the sequences in (\mathbf{c}, \mathbf{d}) are interchanged, the number of bits can be increased to 11 bits. Note that modifying \mathbf{c} and \mathbf{d} does not destroy the orthogonality between the sequences for different users as $\mathbf{a} \odot \mathbf{s}_r$ and $\mathbf{b} \odot \mathbf{s}_r$ are multiplied with scalars depending on the elements of \mathbf{c} , \mathbf{d} , $\tilde{\mathbf{c}}$, and $\tilde{\mathbf{d}}$.

In Figure 5, we illustrate how \mathbf{a} and \mathbf{b} are placed in each PRB and modified based on $f_i(\mathbf{x})$ and $f_o(\mathbf{x}, z)$ for $N_{rb} = 10$ with the proposed scheme. Interchanging \mathbf{a} and \mathbf{b} , the values of π and ϕ are controlled with 3 UCI bits. The output of the order encoder is exemplified for $\pi = (3, 2, 1)$ and $\phi = (3, 1, 2)$,

which gives $(\mathbf{c}, \mathbf{d}, \tilde{\mathbf{c}}, \tilde{\mathbf{d}}, \mathbf{c}, \mathbf{d}, \tilde{\mathbf{c}}, \tilde{\mathbf{d}})$. The parameters $c_{n=1,2,3}, c' \in \mathbb{Z}_4$ are set based on 8 UCI bits. The bit mapping is done based on a Gray mapping, e.g., $00 \rightarrow 0$, $01 \rightarrow 1$, $10 \rightarrow 3$, and $11 \rightarrow 2$, to improve the error rate performance. Since the output of the RM code over \mathbb{Z}_4 is distributed to 5 different PRBs as in Figure 5, the proposed scheme inherently exploits the frequency diversity in the frequency selective channels.

2) *Receiver Design*: The proposed scheme is compatible with the RM code in [18]. Thus, a simple receiver can be developed by re-using the maximum-likelihood (ML) decoder proposed in [29] for first-order RM codes. At the receiver, we first separate the users by applying the matched filters for $\mathbf{a} \odot \mathbf{s}_r$ and $\mathbf{b} \odot \mathbf{s}_r$ for different r , which lead to 4 complex values for each PRB and user. We then coherently combine $N_{rb}/2$ complex values distributed to $N_{rb}/2$ different PRBs based on maximum-ratio combining (MRC). Subsequently, we use the ML decoder in [29] to obtain $c_{n=1,2,3}$ and c' . We perform this operation for 8 different hypotheses due to the combinations of interchange of \mathbf{a} and \mathbf{b} , π , and ϕ . We choose the best hypothesis based on ML.

The receiver for this scheme requires the estimate of the channel between the receiver and each user. The channel estimation for multiple users can be achieved by using a dedicated OFDM symbol constructed with the proposed scheme with a set of fixed parameters. Since $\{\mathbf{a} \odot \mathbf{s}_0, \mathbf{a} \odot \mathbf{s}_1, \mathbf{a} \odot \mathbf{s}_2\}$ and $\{\mathbf{b} \odot \mathbf{s}_0, \mathbf{b} \odot \mathbf{s}_1, \mathbf{b} \odot \mathbf{s}_2\}$ are orthogonal sets, the receiver can estimate the channel for each user with a set of matched filters in the frequency domain for fixed π , ϕ , \mathbf{c} , \mathbf{d} , c_n and c' .

Our receiver introduces $N_{rb}N_{sc} + 8 \times N_{rb}N_{sc}/3$ complex multiplications and $2/3N_{rb}N_{sc} + 8 \times 8(N_{rb}/2 - 1)$ complex summations for the user separation and the hypothesis testing in addition to the complexity of the ML decoder which is low for $m = 3$ as reported in [29].

V. NUMERICAL ANALYSIS

In this section, we evaluate the proposed modulation schemes numerically. We consider the interlace parameters

in NR-U for 15 kHz. For the first scheme, we employ the sequences given in Table I and the spreading sequences $\mathbf{a} = (+, +, +, j, i)$ and $\mathbf{b} = (+, i, -, +, j)$. For comparison, we consider the sequences adopted in [6] for PUCCH Format 0 and 1 and introduce three PAPR minimization techniques for interlaced transmission. The first two methods rely on the optimal phase rotation (i.e., partial transmit sequences (PTS)) with the QPSK alphabet for each PRB for a given sequence, which prioritize either cubic metric (CM) or PAPR. The third approach is *cyclic-shift hopping* adopted in NR for interlaced transmission with PUCCH Format 0 [6]. The sequence on k th occupied PRB in the interlace is multiplied with the sequence $(e^{j\frac{2\pi i}{N_{sc}} \times 0}, e^{j\frac{2\pi i}{N_{sc}} \times 1}, \dots, e^{j\frac{2\pi i}{N_{sc}} \times (N_{sc}-1)})$ for $k = 0, 1, \dots, 9$. For the fourth design, we generate all possible ZC sequences of length 113 (cyclically padded to 120) and select the best 30 sequences based on the PAPR of the corresponding signals after they are mapped to the interlace. For all schemes, we assume that 6 users transmit orthogonal sequences to indicate ACK or NACK on the same interlace as discussed in Section IV-A1.

For a larger UCI payload, we consider the modulation scheme introduced in Section IV-B1 and set $\mathbf{a} = (+, i, +)$, $\mathbf{b} = (+, +, -)$, $\mathbf{c} = (+, +, +, j, i)$, and $\mathbf{d} = (+, i, -, +, j)$. We compare the proposed scheme with two other approaches. The first approach uses OCC on each PRB [13]. For this scheme, we consider 10 QPSK symbols for each user. To reduce the PAPR, each QPSK symbol is multiplied with a distinct column of a DFT matrix of size 12 (i.e., the OCC) and the resulting vectors are mapped to the PRBs of interlace. For the second approach, we consider the approach used in Format 3 in NR for interlaced transmission, i.e., pre-DFT OCC. We first generate 30 $\pi/2$ -BPSK symbols for each user and expand it with an OCC sequence of length 4. After we calculate the DFT of the spread sequence, the output is mapped to the interlace [10]. For the sake of fair comparison, we consider the same spectral efficiency for all schemes and transmit 11 UCI bits per user. For the competing schemes, we use the (32,11) linear block code with the rate matching in [11]. At the receiver side, we assume 2 antennas and the received signals are combined with MRC and processed with minimum mean square error (MMSE) equalizer and ML decoder. The receiver for the proposed scheme is given in Section IV-B2.

A. PAPR/CM Distribution

In Figure 6, the PAPR distributions for all aforementioned approaches are provided. For ACK/NACK indication, the optimal phase rotations prioritizing PAPR and CM for NR sequences result in a maximum PAPR of 5.3 dB and 5.7 dB, respectively, while the ZC sequences limit the PAPR to 6 dB. The cyclic-shift hopping also reduces the maximum PAPR to 6 dB. The PAPR for the schemes in [13] and [10] for 11 UCI bits reach to 8.1 dB and 7.3 dB, respectively. The proposed schemes offer limit the PAPR to 3 dB as they exploit CSs. The PAPR gains with the proposed schemes for up-to 2 UCI bits and 11 UCI bits are in the range of 2.7-3 dB and 4.3-5.1 dB, respectively.

Another metric that characterizes the fluctuation of the resulting signal is the CM. We calculate the CM in dB as

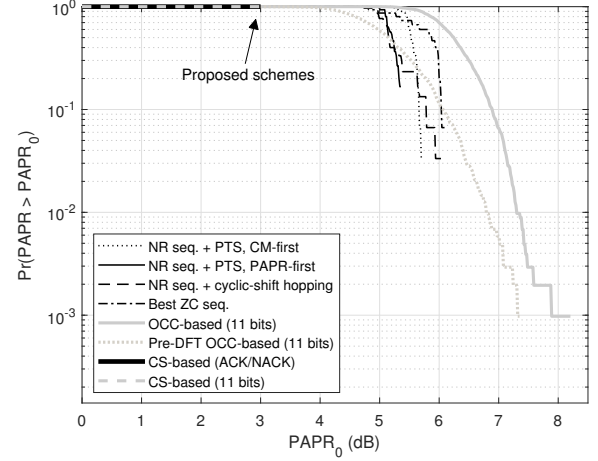


Figure 6. PAPR distribution.

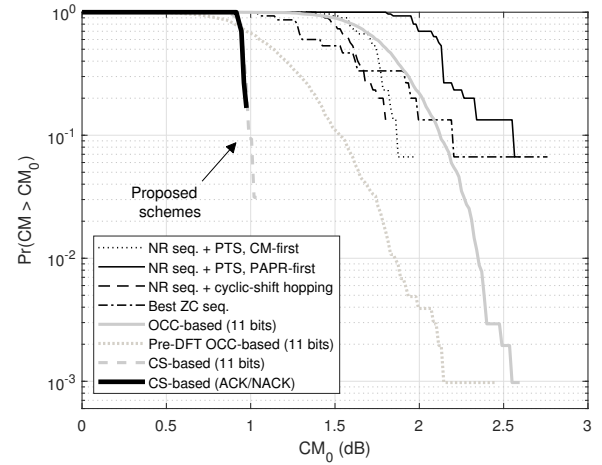


Figure 7. CM distribution.

$CM = 20 \log_{10}(\text{rms}\{v_{\text{norm}}^3(t)\})/1.56$, where $v_{\text{norm}}(t)$ is the synthesized signal in time with the power of 1 [30]. In Figure 7, we compare the CM distributions for the aforementioned schemes. Similar to the PAPR results, the proposed schemes improve the CM within the range of 0.8-1.7 dB over the schemes considered in this study.

B. Peak Cross-correlation Distribution

We evaluate the peak cross-correlation distribution of CSs designed for the first scheme by calculating $\rho_{\text{peak}} = \max\{|\text{IDFT}\{\mathbf{x}_i \odot \mathbf{x}_j^*\}|/N_{\text{sc}}\}$, where \mathbf{x}_i is the i th sequence in the set, $i \neq j$ and $\text{IDFT}\{\cdot, N_{\text{IDFT}}\}$ is the DFT operation of size N_{IDFT} [30]. To achieve a large oversampling in time, we choose $N_{\text{IDFT}} = 4096$. In Figure 8, we provide the distribution of ρ_{peak} for different schemes. The ZC sequences fail as the maximum peak cross-correlation reaches up to 0.95 although 50 percentile performance is better than the other methods. The set of NR sequences results in a maximum of 0.8. On the other hand, they are 0.715 for the both sets \mathcal{C} and \mathcal{D} as we set $\beta = 0.715$. Hence, the proposed set is superior to the sequences adopted in NR in terms of the maximum peak cross-correlation.

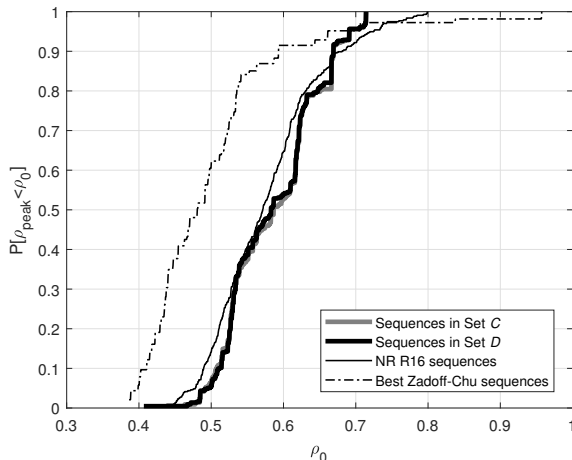


Figure 8. Peak cross-correlation distribution.

C. False Alarm and Miss-Detection Performance

In this analysis, we demonstrate the impact of interlacing on the ACK-to-NACK rate and the ACK miss-detection rate for a given DTX-to-ACK probability. The DTX-to-ACK and NACK-to-ACK rates correspond to the probability of ACK detection when there is no signal or a NACK is being transmitted, respectively. The ACK miss-detection rate is the probability of not detecting ACK when ACK is actually being transmitted. For the single-PRB approach, we consider NR PUCCH Format 0 with interlaced transmission. To show the limits, we consider two extreme channel conditions where the occupied PRBs in an interlace experience the same fading coefficients, i.e., flat fading, or independent-and-identically distributed (i.i.d.) Rayleigh fading to model selective fading. In practice, there is always correlation between channel coefficients. However, the correlation can decrease significantly for a large spacing between the occupied PRBs in an interlace.

In the simulation, we set DTX-to-ACK probability to be 1% at the detector based on Neyman-Pearson criterion and consider MRC of signals from 2 receive antennas. We provide curves based on signal-to-noise ratio (SNR) per subcarrier as it reveals the benefit of interlace under the PSD requirement in the unlicensed band as compared to single PRB transmission. The results in Figure 9 show that the interlaced transmission improves the performance as compared to the single-RB approach due to the increased signal power under the PSD requirement. When the channel is frequency-selective, the slopes of the NACK-to-ACK and ACK miss-detection rates are much larger as the non-contiguous resource allocation exploits the diversity due the frequency selectivity. Note that all the schemes for ACK/NACK indication provide the same error-rate performance. However, the proposed scheme achieves it with low-PAPR and CM, which potentially increases the reliability in unlicensed channels for cell-edge users.

D. Error-rate Comparison

In Figure 10(a) and Figure 10(b), we compare the bit-error rate (BER) and block-error rate (BLER) performance of the second proposed modulation scheme and the methods in

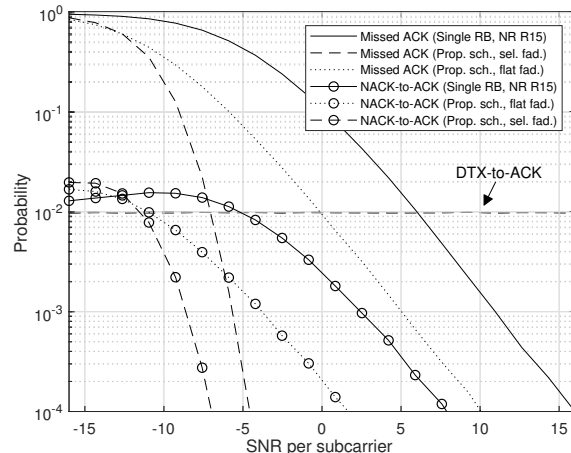


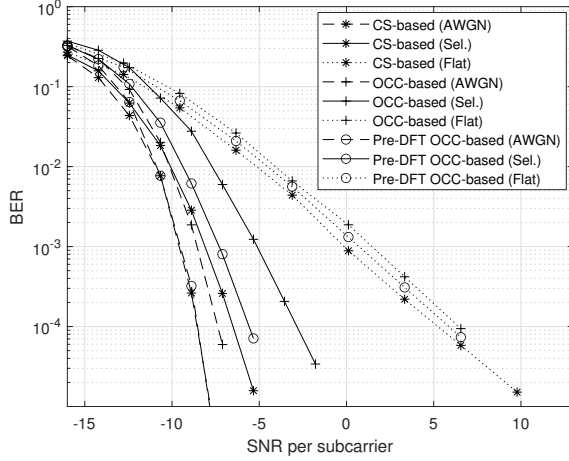
Figure 9. The receiver performance for ACK/NACK transmission.

[10] and [13] for moderate UCI payload. While the minimum Euclidean distance between sequences are 11.3137 and 9.798 for the pre-DFT OCC-based and the OCC-based approaches, respectively, it is 10.9545 for the proposed scheme. Hence, for additive white Gaussian noise (AWGN) channel, the pre-DFT OCC-based scheme [10] offers approximately 0.3 dB and 1 dB gain as compared to proposed scheme and OCC-based scheme, respectively. For flat-fading, the difference between the schemes is negligible at 0.01 BLER. On the other hand, for selective channels, the proposed approach is 2 dB better than the OCC-based scheme and similar to the one in [10], respectively. The performance difference between the proposed method and OCC-based scheme is because the receiver for the proposed scheme coherently combine the symbols on different PRBs with MRC. The receiver for OCC-based scheme cannot exploit the frequency selectivity as the data symbols are not spread to different PRBs. However, the pre-DFT OCC spreads the information to different PRBs through DFT operation and harnesses the selectivity better. However, it does not maintain the flatness in the frequency and frequency-domain equalization (FDE) slightly deteriorates its performance.

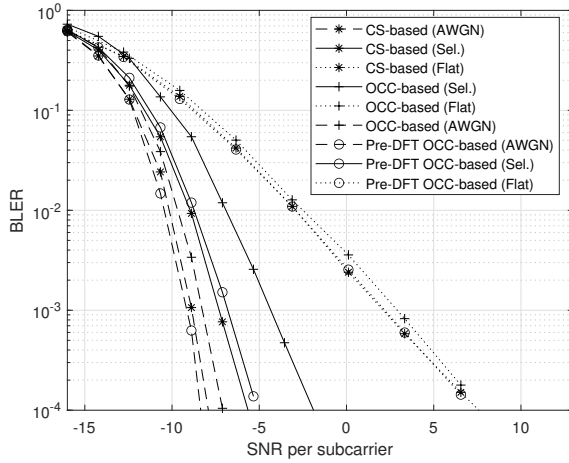
VI. CONCLUDING REMARKS

In this study, we propose two modulation schemes for UL control channels which consist of non-contiguous PRBs in the frequency by exploiting GCPs and introduce Theorem 1 and Theorem 2. The main benefit of the proposed approaches is that they address the PAPR problem of OFDM signals while allowing a flexible non-contiguous resource allocation. For example, the number of null symbols between the PRBs or the number of PRBs in an interlace can be chosen flexibly with minor modifications in both proposed schemes. In all cases, the PAPR of the corresponding signal is less than or equal to 3 dB. With comprehensive numerical analysis, we show that the PAPR gains are in the range of 2.7-3 dB and 4.3-5.1 dB for the first scheme and the second scheme, respectively, as compared other schemes considered in this study.

The first modulation scheme is similar to the NR PUCCH Format 0 for 1 or 2 UCI bits. It separates the PAPR and



(a) BER.



(b) BLER.

Figure 10. Error rate comparison of the proposed CS-based scheme, OCC-based scheme [13], and pre-DFT OCC-based schemes [10] for 11 UCI bits.

CCI minimization problems by utilizing the properties of CSs. While the first challenge is solved by choosing the sequences for PRBs as a GCP in the light of Theorem 1, the second problem is addressed by design a set of GCPs with low peak cross-correlation with a search algorithm. While our algorithm generate a set of GCPs better than the sequences in NR in terms of maximum peak cross-correlation, a systematic solution for a GCP set with low peak cross-correlation is still an open problem. For the second scheme, we develop a new theorem, i.e., Theorem 2, which is capable of generating a wide-variety of CSs though multiple seed sequences. It can generate up to $A! \frac{(m!)^2}{(m-B+1)!} H^{m+1}$ distinct CSs, which is a function of the multiplicity and lengths of the seed GCPs. We show that this joint coding-and-modulation scheme allows 3 users to transmit 11 bits on the same interlace while providing 4.3 dB PAPR gain and similar BLER performance as compared to the approach used in NR PUCCH Format 3. Hence, the proposed schemes can be beneficial for cell-edge users and complement the existing approaches in wireless standards.

APPENDIX A PROOF OF THEOREM 2

Proof. By using Theorem 1, a recursion which generates a GCP $(\mathbf{a}^{(m)}, \mathbf{b}^{(m)})$ for $m \geq 1$ can be given by

$$\begin{aligned} p_{\mathbf{a}^{(n)}}(z) &= p_{\mathbf{c}_{\phi_n}}(z) p_{\mathbf{a}^{(n-1)}}(z) + \omega_n p_{\mathbf{d}_{\phi_n}}(z) p_{\mathbf{b}^{(n-1)}}(z) z^{d_n} w^{2^{\psi_n}}, \\ p_{\mathbf{b}^{(n)}}(z) &= p_{\tilde{\mathbf{d}}_{\phi_n}}(z) p_{\mathbf{a}^{(n-1)}}(z) - \omega_n p_{\tilde{\mathbf{c}}_{\phi_n}}(z) p_{\mathbf{b}^{(n-1)}}(z) z^{d_n} w^{2^{\psi_n}}, \end{aligned} \quad (18)$$

where $\mathbf{a}^{(0)} = \mathbf{b}^{(0)} = 1$, $(\mathbf{c}_{\phi_n}, \mathbf{d}_{\phi_n})$ is the ϕ_n th GCP of length $M_{\phi_n} \in \mathbb{Z}^+$, $\omega_n, w \in \{u : u \in \mathbb{C}, |u| = 1\}$ are arbitrary complex numbers of unit magnitude, $d_n \in \mathbb{Z}$ for $n = 1, 2, \dots, m$, and ψ_n is the n th element of the sequence $\psi = (\psi_n)_{n=1}^m$ defined by the permutation of $\{0, 1, \dots, m-1\}$. The recursion in (18) can be re-expressed as

$$\begin{aligned} p^{(n)} &= C_1^{(n)} D_0^{(n)} \tilde{C}_0^{(n)} \tilde{D}_0^{(n)} \Delta_0^{(n)} \Omega_0^{(n)} S_0^{(n)} (p^{(n-1)}) \\ &\quad + C_0^{(n)} D_1^{(n)} \tilde{C}_0^{(n)} \tilde{D}_0^{(n)} \Delta_1^{(n)} \Omega_1^{(n)} S_0^{(n)} (q^{(n-1)}) w^{2^{\psi_n}}, \\ q^{(n)} &= C_0^{(n)} D_0^{(n)} \tilde{C}_0^{(n)} \tilde{D}_1^{(n)} \Delta_0^{(n)} \Omega_0^{(n)} S_0^{(n)} (p^{(n-1)}) \\ &\quad + C_0^{(n)} D_0^{(n)} \tilde{C}_1^{(n)} \tilde{D}_0^{(n)} \Delta_1^{(n)} \Omega_1^{(n)} S_1^{(n)} (q^{(n-1)}) w^{2^{\psi_n}}, \end{aligned} \quad (19)$$

where $p^{(0)} = q^{(0)} = 1$, the operators $C_0^{(n)}(r)$, $D_0^{(n)}(r)$, $\tilde{C}_0^{(n)}(r)$, $\tilde{D}_0^{(n)}(r)$, $\Delta_0^{(n)}(r)$, $S_0^{(n)}(r)$, $\Omega_0^{(n)}(r)$ are equal to r , and the operators $C_1^{(n)}(r)$, $D_1^{(n)}(r)$, $\tilde{C}_1^{(n)}(r)$, $\tilde{D}_1^{(n)}(r)$, $\Delta_1^{(n)}(r)$, $\Omega_1^{(n)}(r)$, $S_1^{(n)}(r)$ are set to $p_{\mathbf{c}_{\phi_n}}(z)r$, $p_{\mathbf{d}_{\phi_n}}(z)r$, $p_{\tilde{\mathbf{c}}_{\phi_n}}(z)r$, $p_{\tilde{\mathbf{d}}_{\phi_n}}(z)r$, and $z^{d_n}r$, $\xi^{j c_n}r$, and $\xi^{j \frac{H}{2}}r$, respectively.

By utilizing an approach that represents the outcome of a recursion concisely [21] (summarized in Appendix B for the sake of completeness) and investigating the position of the operators in (19), we obtain the configuration vectors, i.e., \mathbf{b}_n^T for $n = 1, 2, \dots, m$, for $C_{0,1}^{(n)}(r)$, $D_{0,1}^{(n)}(r)$, $\tilde{C}_{0,1}^{(n)}(r)$, and $\tilde{D}_{0,1}^{(n)}(r)$ as $[1 \ 0 \ 0 \ 0]$, $[0 \ 1 \ 0 \ 0]$, $[0 \ 0 \ 0 \ 1]$, and $[0 \ 0 \ 1 \ 0]$, respectively. Therefore, by plugging the configuration vectors into (23) and (24), the Boolean functions associated with the construction sequences (or indication sequences) for $C_{0,1}^{(n)}(r)$ are obtained as

$$f_{c,n}(\mathbf{x}) = \begin{cases} (1 - x_{\pi_n}) & n = m \\ (1 - x_{\pi_n})(1 - x_{\pi_{n+1}}) & n < m \end{cases},$$

$$g_{c,n}(\mathbf{x}) = \begin{cases} 0 & n = m \\ (1 - x_{\pi_n})(1 - x_{\pi_{n+1}}) & n < m \end{cases},$$

respectively. Similarly, for $D_{0,1}^{(n)}(r)$,

$$f_{d,n}(\mathbf{x}) = \begin{cases} x_{\pi_n} & n = m \\ x_{\pi_n}(1 - x_{\pi_{n+1}}) & n < m \end{cases},$$

$$g_{d,n}(\mathbf{x}) = \begin{cases} 0 & n = m \\ x_{\pi_n}(1 - x_{\pi_{n+1}}) & n < m \end{cases}.$$

For $\tilde{D}_{0,1}^{(n)}(r)$,

$$f_{\tilde{d},n}(\mathbf{x}) = \begin{cases} 0 & n = m \\ (1 - x_{\pi_n})x_{\pi_{n+1}} & n < m \end{cases},$$

$$g_{\tilde{d},n}(\mathbf{x}) = \begin{cases} (1 - x_{\pi_n}) & n = m \\ (1 - x_{\pi_n})x_{\pi_{n+1}} & n < m \end{cases}.$$

For $\tilde{C}_{0,1}^{(n)}(r)$,

$$f_{\tilde{c},n}(\mathbf{x}) = \begin{cases} 0 & n = m \\ x_{\pi_n}x_{\pi_{n+1}} & n < m \end{cases},$$

$$g_{\tilde{c},n}(\mathbf{x}) = \begin{cases} x_{\pi_n} & n = m \\ x_{\pi_n}x_{\pi_{n+1}} & n < m \end{cases}.$$

Therefore, the combined effects of the operators $C_{0,1}^{(n)}(r)$, $D_{0,1}^{(n)}(r)$, $\tilde{C}_{0,1}^{(n)}(r)$, and $\tilde{D}_{0,1}^{(n)}(r)$ on the coefficients of w^x of $p^{(n)}$ and $q^{(n)}$ can be calculated as

$$\begin{aligned} F_{\text{cd}\tilde{\text{c}}\tilde{\text{d}},x}(r) &= r \prod_{n=1}^m p_{c_{\phi_n}}(z)^{f_{c,n}(\mathbf{x})} p_{\tilde{c}_{\phi_n}}(z)^{f_{\tilde{c},n}(\mathbf{x})} \\ &\quad \times p_{d_{\phi_n}}(z)^{f_{d,n}(\mathbf{x})} p_{\tilde{d}_{\phi_n}}(z)^{f_{\tilde{d},n}(\mathbf{x})} \\ &\stackrel{(a)}{=} r \prod_{n=1}^m p_{c_{\phi_n}}(z)^{f_{c,n}(\mathbf{x})} + p_{\tilde{c}_{\phi_n}}(z)^{f_{\tilde{c},n}(\mathbf{x})} \\ &\quad + p_{d_{\phi_n}}(z)^{f_{d,n}(\mathbf{x})} + p_{\tilde{d}_{\phi_n}}(z)^{f_{\tilde{d},n}(\mathbf{x})} \\ &= r \times f_o(\mathbf{x}, z). \end{aligned}$$

and

$$\begin{aligned} G_{\text{cd}\tilde{\text{c}}\tilde{\text{d}},x}(r) &= r \prod_{n=1}^m p_{c_{\phi_n}}(z)^{g_{c,n}(\mathbf{x})} p_{\tilde{c}_{\phi_n}}(z)^{g_{\tilde{c},n}(\mathbf{x})} \\ &\quad \times p_{d_{\phi_n}}(z)^{g_{d,n}(\mathbf{x})} p_{\tilde{d}_{\phi_n}}(z)^{g_{\tilde{d},n}(\mathbf{x})} \\ &\stackrel{(b)}{=} r \prod_{n=1}^m p_{c_{\phi_n}}(z)^{g_{c,n}(\mathbf{x})} + p_{\tilde{c}_{\phi_n}}(z)^{g_{\tilde{c},n}(\mathbf{x})} \\ &\quad + p_{d_{\phi_n}}(z)^{g_{d,n}(\mathbf{x})} + p_{\tilde{d}_{\phi_n}}(z)^{g_{\tilde{d},n}(\mathbf{x})} \\ &= r \times g_o(\mathbf{x}, z), \end{aligned}$$

respectively, where (a) ((b)) is because only one of the functions among $f_{c,n}(\mathbf{x})$, $f_{\tilde{c},n}(\mathbf{x})$, $f_{d,n}(\mathbf{x})$, and $f_{\tilde{d},n}(\mathbf{x})$ ($g_{c,n}(\mathbf{x})$, $g_{\tilde{c},n}(\mathbf{x})$, $g_{d,n}(\mathbf{x})$, and $g_{\tilde{d},n}(\mathbf{x})$) is 1 while the others are equal to 0.

By defining $\omega_n \triangleq \xi^{jc_n}$ and using the identity $\xi^{j\frac{H}{2}} = -1$, the coefficients of w^x of $p^{(n)}$ and $q^{(n)}$ due to the operators $S_{0,1}^{(n)}(r)$, $\Omega_{0,1}^{(n)}(r)$, and $\Delta_{0,1}^{(n)}(r)$ are obtained in [21]. Their compositions can be expressed as $F_{\text{comp},x}(r) = G_{\text{comp},x}(r) = r\xi^{jc_i(\mathbf{x})} \times z^{f_s(\mathbf{x})}$. Finally, by composing $F_{\text{cd}\tilde{\text{c}}\tilde{\text{d}},x}(r)$ and $F_{\text{comp},x}(r)$, and $G_{\text{cd}\tilde{\text{c}}\tilde{\text{d}},x}(r)$ and $G_{\text{comp},x}(r)$, $p_{\mathbf{b}^{(m)}}(z)$ and $p_{\mathbf{b}^{(m)}}(z)$ can be calculated as

$$\begin{aligned} p_{\mathbf{b}^{(m)}}(z) &= p^{(m)} \\ &= \sum_{x=0}^{2^m-1} F_{\text{cd}\tilde{\text{c}}\tilde{\text{d}},x}(F_{\text{comp},x}(r))w^x \Big|_{r=p^{(0)}=q^{(0)}=1} \\ &= \sum_{x=0}^{2^m-1} f_o(\mathbf{x}, z) \times \xi^{jc_i(\mathbf{x})} \times z^{f_s(\mathbf{x})} \times w^x \end{aligned}$$

and

$$\begin{aligned} p_{\mathbf{b}^{(m)}}(z) &= q^{(m)} \\ &= \sum_{x=0}^{2^m-1} G_{\text{cd}\tilde{\text{c}}\tilde{\text{d}},x}(G_{\text{comp},x}(r))w^x \Big|_{r=p^{(0)}=q^{(0)}=1} \\ &= \sum_{x=0}^{2^m-1} g_o(\mathbf{x}, z) \times \xi^{jc_i(\mathbf{x})} \times z^{f_s(\mathbf{x})} \times w^x, \end{aligned}$$

respectively, where w can be chosen arbitrarily as $w = z^U$.

The sequences $\mathbf{a}^{(m)}$ and $\mathbf{b}^{(m)}$ construct a GCP based on (18). Since the phase rotation does not change the APAC of a sequence, $\mathbf{a}^{(m)} \times \xi^{jc'}$ and $\mathbf{b}^{(m)} \times \xi^{jc''}$ also construct a GCP. \square

APPENDIX B

REPRESENTATION OF A RECURSION

For $n = 1, 2, \dots, m$, consider a recursion given by

$$\begin{aligned} p^{(n)} &= \mathcal{O}_{11}^{(n)}(p^{(n-1)}) + \mathcal{O}_{12}^{(n)}(q^{(n-1)})w^{2^{\psi_n}}, \\ q^{(n)} &= \mathcal{O}_{21}^{(n)}(p^{(n-1)}) + \mathcal{O}_{22}^{(n)}(q^{(n-1)})w^{2^{\psi_n}}, \end{aligned} \quad (20)$$

where w is an arbitrary complex number, ψ_n is the n th element of the sequence $\boldsymbol{\psi} \triangleq (\psi_n)_{n=1}^m$ defined by the permutation of $\{0, 1, \dots, m-1\}$, $\mathcal{O}_{ij}^{(n)} \in \{\mathcal{O}_0^{(n)}, \mathcal{O}_1^{(n)}\}$ is a linear operator which transforms one function to another function in \mathcal{F} , and $p^{(0)} = q^{(0)} = r$. In [21], it was shown that $p^{(m)}$ and $q^{(m)}$ can be obtained as

$$p^{(m)} = \sum_{x=0}^{2^m-1} \overbrace{\mathcal{O}_{f_m(x)}^{(m)} \cdots \mathcal{O}_{f_n(x)}^{(n)} \cdots \mathcal{O}_{f_2(x)}^{(2)} \mathcal{O}_{f_1(x)}^{(1)}(r)}^{F_x(r)} w^x, \quad (21)$$

and

$$q^{(m)} = \sum_{x=0}^{2^m-1} \overbrace{\mathcal{O}_{g_m(x)}^{(m)} \cdots \mathcal{O}_{g_n(x)}^{(n)} \cdots \mathcal{O}_{g_2(x)}^{(2)} \mathcal{O}_{g_1(x)}^{(1)}(r)}^{G_x(r)} w^x, \quad (22)$$

where

$$f_n(\mathbf{x}) = \begin{cases} b_{11}^{(n)}(1 - x_{\pi_n}) + b_{12}^{(n)}x_{\pi_n} & n = m \\ b_{11}^{(n)}(1 - x_{\pi_n})(1 - x_{\pi_{n+1}}) \\ \quad + b_{12}^{(n)}x_{\pi_n}(1 - x_{\pi_{n+1}}) \\ \quad + b_{21}^{(n)}(1 - x_{\pi_n})x_{\pi_{n+1}} \\ \quad + b_{22}^{(n)}x_{\pi_n}x_{\pi_{n+1}} & n < m \end{cases}, \quad (23)$$

$$g_n(\mathbf{x}) = \begin{cases} b_{21}^{(n)}(1 - x_{\pi_n}) + b_{22}^{(n)}x_{\pi_n} & n = m \\ b_{11}^{(n)}(1 - x_{\pi_n})(1 - x_{\pi_{n+1}}) \\ \quad + b_{12}^{(n)}x_{\pi_n}(1 - x_{\pi_{n+1}}) \\ \quad + b_{21}^{(n)}(1 - x_{\pi_n})x_{\pi_{n+1}} \\ \quad + b_{22}^{(n)}x_{\pi_n}x_{\pi_{n+1}} & n < m \end{cases}, \quad (24)$$

for $n = 1, 2, \dots, m$, where $\pi_n = m - \psi_n$ is the n th element of the sequence $\boldsymbol{\pi} \triangleq (\pi_n)_{n=1}^m$, $b_{ij}^{(n)} = 0$ if $\mathcal{O}_{ij}^{(n)} = \mathcal{O}_0^{(n)}$ and $b_{ij}^{(n)} = 1$ if $\mathcal{O}_{ij}^{(n)} = \mathcal{O}_1^{(n)}$. The vector $\mathbf{b}_n = [b_{11}^{(n)} \ b_{12}^{(n)} \ b_{21}^{(n)} \ b_{22}^{(n)}]$ is denoted as the configuration vector.

The functions $f_n(\mathbf{x})$ and $g_n(\mathbf{x})$ show which of the two operators, i.e., $\mathcal{O}_0^{(n)}$ and $\mathcal{O}_1^{(n)}$, are involved in the construction of

$F_x(r)$ and $G_x(r)$ by setting the indices as $O_{f_n(x)}^{(n)}$ and $O_{g_n(x)}^{(n)}$, respectively. The binary sequences associated with $f_n(x)$ and $g_n(x)$ are referred to as the n th construction sequences (or indication sequences) of $p^{(m)}$ and $q^{(m)}$ for $n = 1, 2, \dots, m$.

REFERENCES

- [1] A. Sahin and R. Yang, "A reliable uplink control channel design with complementary sequences," in *Proc. IEEE International Conference on Communications (ICC)*, May 2019.
- [2] S. Lagen, L. Giupponi, S. Goyal, N. Patriciello, B. Bojović, A. Demir, and M. Beluri, "New radio beam-based access to unlicensed spectrum: Design challenges and solutions," *IEEE Commun. Surveys Tuts.*, vol. 22, no. 1, pp. 8–37, 2020.
- [3] M. Labib, V. Marojevic, J. H. Reed, and A. I. Zaghloul, "Extending LTE into the unlicensed spectrum: Technical analysis of the proposed variants," *IEEE Communications Standards Magazine*, vol. 1, no. 4, pp. 31–39, Dec. 2017.
- [4] A. Aijaz, H. Aghvami, and M. Amani, "A survey on mobile data offloading: technical and business perspectives," *IEEE Wireless Commun.*, vol. 20, no. 2, pp. 104–112, Apr. 2013.
- [5] ETSI, "5 GHz RLAN; Harmonized EN covering the essential requirements of article 3.2 of the Directive 2014/53/EU," EN 301 893, May 2017.
- [6] 3GPP, "Physical channels and modulation (Release 16)," TS 38.211 V16.0.0, Dec. 2019.
- [7] —, "Physical channels and modulation (Release 15)," TS 38.211 V15.0.0, Mar. 2017.
- [8] L. Kundu, G. Xiong, and J. Cho, "Physical uplink control channel design for 5G New Radio," in *Proc. IEEE 5G World Forum (5GWF)*, Jul. 2018, pp. 233–238.
- [9] J. J. Benedetto, I. Konstantinidis, and M. Rangaswamy, "Phase-coded waveforms and their design," *IEEE Signal Processing Magazine*, vol. 26, no. 1, pp. 22–31, Jan. 2009.
- [10] Qualcomm, "UL signals and channels for NR-U," R1-183412, Nov. 2018.
- [11] 3GPP, "Multiplexing and channel coding (Release 16)," TS 38.212 V16.0.0, Dec. 2019.
- [12] Ericsson, "UL signals and channels for NR-U," R1-1907453, May 2019.
- [13] —, "UL signals and channels for NR-U," R1-1900997, Jan. 2019.
- [14] —, "Feature lead summary for UL signals and channels," R1-1912715, Aug. 2019.
- [15] Y. Rahmatallah and S. Mohan, "Peak-to-average power ratio reduction in OFDM systems: A survey and taxonomy," *IEEE Commun. Surveys Tut.*, vol. 15, no. 4, pp. 1567–1592, Fourth 2013.
- [16] G. Wunder, R. F. H. Fischer, H. Boche, S. Litsyn, and J. No, "The PAPR problem in OFDM transmission: New directions for a long-lasting problem," *IEEE Signal Processing Magazine*, vol. 30, no. 6, pp. 130–144, Nov. 2013.
- [17] H. G. Myung, J. Lim, and D. J. Goodman, "Single carrier FDMA for uplink wireless transmission," *IEEE Vehicular Technology Magazine*, vol. 1, no. 3, pp. 30–38, Sep. 2006.
- [18] J. A. Davis and J. Jedwab, "Peak-to-mean power control in OFDM, Golay complementary sequences, and Reed-Muller codes," *IEEE Trans. Inf. Theory*, vol. 45, no. 7, pp. 2397–2417, Nov. 1999.
- [19] M. Golay, "Complementary series," *IRE Trans. Inf. Theory*, vol. 7, no. 2, pp. 82–87, Apr. 1961.
- [20] Y. Hori and H. Ochiai, "A new uplink multiple access based on ofdm with low papr, low latency, and high reliability," *IEEE Transactions on Communications*, vol. 66, no. 5, pp. 1996–2008, Jun 2018.
- [21] A. Sahin and R. Yang, "A generic complementary sequence encoder," *CoRR*, vol. abs/1810.02383v2, Aug. 2019.
- [22] M. G. Parker, K. G. Paterson, and C. Tellambura, "Golay complementary sequences," in *Wiley Encyclopedia of Telecommunications*, 2003.
- [23] S. Sesia, I. Toufik, and M. Baker, *LTE, The UMTS Long Term Evolution: From Theory to Practice*. Wiley Publishing, 2009.
- [24] R. Turyn, "Hadamard matrices, Baumert-Hall units, four-symbol sequences, pulse compression, and surface wave encodings," *Journal of Combinatorial Theory, Series A*, vol. 16, no. 3, pp. 313–333, 1974.
- [25] E. Garcia, J. J. Garcia, J. U. A. M. C. Perez, and A. Hernandez, "Generation algorithm for multilevel LS codes," *Electronics Letters*, vol. 46, no. 21, pp. 1465–1467, Oct. 2010.
- [26] K. G. Paterson, "Generalized Reed-Muller codes and power control in OFDM modulation," *IEEE Trans. Inf. Theory*, vol. 46, no. 1, pp. 104–120, Jan. 2000.
- [27] W. H. Holzmann and H. Kharaghani, "A computer search for complex Golay sequences," *Aust. Journ. Comb.*, vol. 10, pp. 251–258, Apr. 1994.
- [28] InterDigital, "Evaluation of CGS candidates for PUCCH," R1-1718490, Oct. 2017.
- [29] K. Schmidt and A. Finger, "Simple maximum-likelihood decoding of generalized first-order Reed-Muller codes," *IEEE Communications Letters*, vol. 9, no. 10, pp. 912–914, Oct. 2005.
- [30] Ericsson, Nokia, Lenovo, LG, and ZTE, "WF on DMRS multi-tone evaluation methods," R1-163437, Apr. 2016.